Morphological instability and dynamics of fronts in bacterial growth models with nonlinear diffusion

Judith Müller* and Wim van Saarloos
Instituut–Lorentz, Universiteit Leiden, Postbus 9506, 2300 RA Leiden, The Netherlands
(Received 26 November 2001; published 28 June 2002)

Depending on the growth condition, bacterial colonies can exhibit different morphologies. As argued by Ben-Jacob *et al.* there is biological and modeling evidence that a nonlinear diffusion coefficient of the type $D(b)=D_0 b^k$ is a basic mechanism that underlies almost all of the patterns and generates a long-wavelength instability. We study a reaction-diffusion system with a nonlinear diffusion coefficient and find that a unique planar traveling front solution exists whose velocity is uniquely determined by k and $D=D_0/D_n$, where D_n is the diffusion coefficient of the nutrient. Due to the fact that the bacterial diffusion coefficient vanishes when $b\to 0$, in the front solution b vanishes in a singular way. As a result the standard linear stability analysis for fronts cannot be used. We introduce an extension of the stability analysis that can be applied to singular fronts, and use the method to perform a linear stability analysis of the planar bacteriological growth front. We show that a nonlinear diffusion coefficient generates a long-wavelength instability for $k>0$ and $D<D_c(k)$. We map out the region of stability in the D-k-plane and determine the onset of stability that is given by $D_c(k)$. Both, for $D\to 0$ and $k\to\infty$ the dynamics of the growth zone essentially reduces to that of a sharp interface problem that is reminiscent of a so-called one-sided growth problem where the growth velocity is proportional to the gradient of a diffusion field ahead of the interface. The moving boundary approximation that we derive in these limits is quite accurate but surprisingly does not become a proper asymptotic theory in the strict mathematical sense in the limit $D\to 0$, due to lack of full separation of scales on all dynamically relevant length scales. Our linear stability analysis and sharp interface formulation will also be applicable to other examples of interface formation due to nonlinear diffusion, like in porous media or in the problem of vortex motion in superconductors.

DOI: 10.1103/PhysRevE.65.061111 PACS number(s): 05.40.−a, 05.70.Ln, 81.10.Aj, 87.10.+e

I. INTRODUCTION

A. Background of the problem

Recently the growth of bacterial colonies under different growth conditions has been the focus of attention of several groups in the physics community since it exhibits different elaborate branching patterns. For an extensive review and entrance to the literature, see [1–3]. Already in 1989, Fujikawa and Matsushita [4] stressed that bacterial colonies could grow patterns similar to the type known from the study of physical systems such as diffusion-limited aggregation. A complete morphology diagram has been obtained for the colonies of *Bacillus subtilis* [1,5,6], where the important control parameters are agar concentration that influences the diffusion of the bacteria as well as of the nutrient, and the initial nutrient concentration. It includes some interesting regimes such as diffusion limited aggregation, dense branching morphologies, and Eden-like and ring patterns. Although the visual appearance of the patterns is very similar to those of physical systems, at the microscopic level their growth mechanism has to be different—the question then becomes whether or not these microscopic differences affect the overall large-scale pattern dynamics. For instance, the building units are bacteria that are themselves micro-organisms and thus living systems. To survive they have to cope with hostile environmental conditions that made them develop quite sophisticated cooperation mechanisms and communication skills, such as direct cell-cell interaction via extramembrane polymers, collective production of extracellular ''wetting'' fluid for movement on hard surfaces, long-range chemical signaling, such as quorum sensing and chemotactic signaling, just to name a few. Different models have been proposed that include one or several of these mechanisms, and are able to reproduce the rich morphology diagram quite well. Instead of exploring the richness and diversity of the behavior of bacterial colonies, we want to concentrate on the basic mechanism that underlies all these patterns. Since they appear as an interface separating a region occupied by the bacteria from a bacteria-free region, which propagates as the colony is expanding, we look for an interface model that includes a long-wavelength instability. Although these models have been developed and studied for pattern forming, nonliving systems such as crystal growth [7–9], where a sharp-interface formulation is well justified, even at quite small length scales, here the existence of interface-type fronts is not obvious from the start, but is something that should emerge from the continuum equations describing the dynamics. Reaction-diffusion-type models with a nonlinear diffusion coefficient for the bacteria density have been argued to be a good candidate for being the proper starting point to analyze the instability mechanism since they were able to reproduce many aspects of the above-mentioned morphology diagram [2,10–13].

The biological motivation that has been proposed for nonlinear diffusion coefficient is the way bacteria move. Although there are different ways of moving we are interested

*Present address: DigitalDNA Laboratories, Motorola, Austin, TX 78721.

 ©2002 The American Physical Society

in bacteria that swim by propelling themselves with their flagella in straight lines and change their direction in a random fashion by tumbling that can be described by a random walk. However, for the propelling mechanism to work a liquid with low viscosity is required. Since bacteria by themselves are able to secrete this liquid, their presence is required to generate the lubricant layer necessary for diffusion. This behavior can be captured qualitatively by a bacteria-density-dependent diffusion coefficient as has been proposed in particular by Ben-Jacob and co-workers in Ref. [11]. A consequence of it is that the branches of bacterial colonies are confined by a sharp envelope that is supported by the observation with optical microscopes [2,11].

However, we would like to note that the arguments supporting a nonlinear diffusion model are still not conclusive and more of a qualitative nature. In addition, it is clear that it does not appear to be relevant for the growth patterns at large agar concentrations where the bacteria are nonmotile [6], and the relevance for the regions where bacteria are motile is still under discussion. In this paper we will not address the question of the biological relevance of the model; instead we aim to contribute to the debate by working out the stability diagram and uncovering its essential dynamics. An additional nonbiological contribution of our paper is that we introduce new methods to mathematically deal with singular fronts. As we discuss below, this is likely to have implications in other subfields of physics.

In passing, we also note that it has been shown recently [14] that if one extends the model by introducing an effective cutoff in the reaction term modeling the bacterial growth, while keeping the bacterial diffusion term linear, one also recovers the type of front instability necessary to understand bacterial patterns. The motivation for such a cutoff would be simply the fact that bacteria are discrete entities, so that at some small density a continuum formulation breaks down. The two mechanisms (nonlinear diffusion and discrete entity cutoff effects to continuum formulations) are not mutually exclusive and can be operative simultaneously, but the detailed studies of various models by a number of authors [2,10–13] suggests that the nonlinear diffusion mechanism is the most important one of the two [15].

We concentrate on the effect of a nonlinear diffusion coefficient here since in spite of the suggestion that a nonlinear diffusion coefficient is a possible mechanism to generate the complex morphology diagram, a clear understanding of this instability mechanism is still missing. This is surprising since also from a mathematical point of view it is an interesting problem as it defines a new class of fronts that do show up in other systems with density-dependent diffusivity, such as porous media [16–18], or magnetic flux vortices in superconductors [19,20]. Clearly, understanding the similarities and differences between instabilities in magnetic flux patterns and the well-studied Mullins-Sekerka instability mechanism is clearly of importance. Considering the amount of work and the attention given in the recent years to understand the mechanisms behind bacterial colony growth, it might at first sight seem surprising that not even a stability analysis of planar fronts solutions has been performed. An important reason for this is that as the problem involves singularities: these make the standard stability calculations break down, so new techniques have to be introduced to even perform the linear stability analysis. We have been able to resolve the problem and thus perform an explicit linear stability analysis of planar fronts, which allows us to determine the regions of stability in parameter space. Our extension of the standard stability calculation is not limited to the particular bacterial growth problem we focus on here. Instead it should be applicable to a large class of growth problems with singular fields, e.g., other problems that involve nonlinear diffusion, like the vortex patterns in superconductors [19,20] just mentioned, should be amenable to the same type of analysis.

In some limits, in particular in the limit that the bacterial diffusion coefficient becomes much smaller than the one of the nutrient, the fronts in the models that have been studied become rather sharp. A second important question therefore is to what extent a moving boundary approximation, in which the front is viewed as a mathematically sharp interface on the scale of the patterns, becomes appropriate—such approximations are often very helpful for analyzing pattern forming problems (see, e.g., [21] for an application to dendritic growth and an entry into the vast ''phase field model'' literature). Some steps in this direction for the bacterial growth problem were taken by Kitsunezaki [22]. We address this question in more detail in this paper and, quite remarkably, find that while in the limit of small bacterial diffusion a moving boundary approximation is quite accurate, it does not emerge as the lowest-order description in a mathematically well-defined limit. The reason for this is that even for small diffusion, the dynamically relevant length scales (i.e., those corresponding to unstable modes in the linear stability calculation of planar fronts) are not all large in comparison with the front width. This result shows that bacterial growth problems with nonlinear diffusion of the type encountered in the porous media equation [16,18] are mathematically in some crucial ways different from the standard type of growth problems. Physically, their dynamics is closest to those of the so-called one-sided growth problems [7].

B. The model

Since we would like to concentrate on the basic mechanism that generates a long-wavelength instability, we confine our analysis to the most basic model of Ben-Jacob and coworkers [10,11], namely, a two-dimensional reaction-diffusion system for the bacteria density $b(\mathbf{r},t)$ with a nonlinear diffusion term, and the nutrient density $n(\mathbf{r},t)$ with a linear diffusion term:

$$\frac{\partial b}{\partial t} = \nabla D(b) \nabla b + f(n,b), \tag{1}$$

$$\frac{\partial n}{\partial t} = D_n \nabla^2 n - g(n,b), \tag{2}$$

with D_n describing the diffusion constant of the nutrient, and

$$D(b) = D_0 b^k \tag{3}$$

implying a bacteria-density-dependent diffusion coefficient as was motivated before. For simplicity we assume the following reaction term,

$$f(n,b)=g(n,b)=nb, \tag{4}$$

which in chemical terms is like a bilinear autocatalytic reaction,

$$N+B\rightarrow 2B. \tag{5}$$

Biologically it models that the bacteria B eat a nutrient N to duplicate themselves. This involves a conservation law and is clearly an oversimplification, since part of the energy is also used for movement and other metabolic activities. For the growth process we want to study here, this should not matter. For the same reason, we also leave out in this paper another biologically important feature, sporulation, a transition of motile bacteria into a stationary state; this occurs if there is a deficiency of nutrient, which seems to play an important role in the later stage of the branching process. During sporulation bacteria stop normal activity such as movement and use all their internal reserves to metamorphose from an active motile cell to a spore, a sedentary durable ''seed'' that is immotile and hence cannot participate in the diffusion process. The sporulation process can be included in the model by adding a term $-\mu b$ on the right-hand side of Eq. (1). Although the simulation by Kitsunezaki [22] indicates that this death term does affect the stability of planar fronts, we will not take it into account here since the most crucial ingredient is the nonlinear diffusion coefficient of b as it assumes that without bacteria there is no diffusion. As we will see this implies a front profile that goes abruptly to zero, with a divergent slope for $k>1$. This characteristic is supported by experimental observations of some kinds of bacteria, where one observes a clearly defined envelope (such a comparison suggests a value of k of about one). The question we want to study now, is whether this kind of diffusion is enough to generate a long-wavelength instability. It should be noted here that for $k=0$ the system has been studied by [23–25]. They showed that bilinear autocatalysis alone is not sufficient to destabilize a planar front. Only in the presence of an autocatalysis term proportional to b^{γ} with $\gamma>1$ and $D_n>\beta_c D_0$, where β_c depends on the amount and order of autocatalysis, a planar front is unstable toward long-wavelength perturbations [15,26,27]. Thus, any instability we observe for $k>0$ is due to the nonlinearity in the diffusion term. By rescaling the diffusion constant $D=D_0/D_n$ and replacing $f(n,b)$ and $g(n,b)$ by Eq. (4), we obtain the following nonlinear reaction-diffusion system,

$$\frac{\partial b}{\partial t}=\frac{D}{k+1}\nabla^2 b^{k+1}+nb, \tag{6}$$

$$\frac{\partial n}{\partial t}=\nabla^2 n-nb, \tag{7}$$

which contains two parameters, D is the rescaled diffusion constant, and k describing the nonlinearity and the stiffness of the front—in writing the above equations, we have used the freedom to choose appropriate time and length scales, and to rescale the fields n and b appropriately to set all other prefactors equal to one. We will be interested in front solutions of this equation where far ahead of the front the nutrient field $n\rightarrow 1$; as we will discuss in more detail below, this asymptotic value is also immaterial, as the problem with another asymptotic value can be rescaled to our problem with a renormalized value of D.

A nonlinear diffusion behavior like in Eq. (6) also arises in the so-called porous media equation [16–18]. There is a vast literature on this equation [16,18]; for us, the essential feature is that it gives rise to moving front solutions with compact support, i.e., for which the field b is zero in some regions of space. At the point where b vanishes, it does so in a singular way, and this invalidates the usual linear stability analysis.

C. Overview of methods and results

For the reader not interested in the mathematical details of the derivation, we now summarize the main results of the analysis. The model (6)-(7) has two homogeneous states: a stable solution $(c_b,0)$ in which only bacteria are present, and an unstable solution $(0,c_n)$ with only nutrient. Thus, we can study the propagation of the stable state $(c_b,0)$ into the unstable one $(0,c_n)$, implying for our system the propagation of the bacteria field into the nutrient field. To study such a propagation we look for one-dimensional traveling front solutions that appear for a system with initial conditions in which the system is in the unstable state and a small perturbation at $x\rightarrow-\infty$ starts to invade it. Assuming that the front propagates with a steady velocity v, we can reformulate the model in a comoving frame that reduces Eqs. (6),(7) to a one-dimensional system of ordinary differential equations (ODEs) that is much easier to analyze. Its solution will be found numerically by a shooting method as will be explained in Sec. II.

We find that there generally is a clearly defined unique reaction front, of which b vanishes with a diverging slope for $k>1$ (see Figs. 5 and 6 below). The qualitative features of these fronts are consistent with the earlier simulation results of Ben-Jacob and co-workers [10,11] and can be traced back to the nonlinear diffusion. The characteristic singular behavior of the front makes the study of the problem mathematically and numerically challenging and intriguing. The solution provides us with a unique velocity, which depends on D and k and is shown in Fig. 1. More detailed plots of the behavior of the velocity as a function of D and k are presented later in Sec. II of this paper.

In order to study the stability of the front that is the content of Sec. III, we have to perturb the planar front. Due to the singular behavior of the planar front a perturbation of the front is not only a simple perturbation in the fields b and n but also in the geometry of the front as sketched in Fig. 2.

Our stability analysis implements the idea that a proper ansatz consists of two contributions, a perturbation in the line of the singular front, and the perturbation in the fields away from the singular line. Both of these contributions have to be determined self-consistently. For $k>0$ we observe that for $D<D_c(k)$ the planar front is unstable and has a long-

wavelength instability. Thus, a nonlinear diffusion coefficient together with a bilinear autocatalysis-type reaction term are sufficient to generate a long-wavelength instability. For $D > D_c(k)$ the planar front is linearly stable. Hence, in the D-k-parameter space there exist regions of stability and instability of a planar front. We determine these regions in two different ways, one by performing numerically a linear stability analysis as is done in Sec. III A, the other by an expansion for small growth rate ω and wave number q around the planar profile as is done in Sec. III C. Figure 3 shows the stability diagram as a function of D and k.

Filled circles show the onset of the region of stability of planar fronts as determined by a numerical linear stability analysis, and filled diamonds show the same boundary as obtained from the exact expression for $d^2\omega/dq^2|_{q=0}$ derived in Sec. III C. Both methods give results that are in very good agreement with each other, as they should. The solid line is there to guide the eye, the dashed line hints to the fact that while we expect the line of $D_c(k)$ to approach the origin we do not know the precise analytic behavior of $D_c(k)$ for $k \to 0$, since for $k=0$ the planar front is stable for all D [23,24]. We will not analyze the precise behavior in the limit $k \to 0$ in detail, both because it does not appear to be of practical relevance, and because the model is very sensitive to slight changes in this limit: an effective cutoff that arises for discrete particle effects turns the model weakly unstable [14], but a continuum model with a different reaction term has the same effect. In particular, if we change the reaction term nb in Eqs. (6),(7) to nb^γ, then for any $\gamma > 1$ we expect for the limit $k \to 0$ D_c to be finite; in other words, for $\gamma > 1$ the stability boundary crosses the D axis at a nonzero value of D. For $\gamma = 2$, it is in fact known that $D_c(k=0) \approx 0.34$ [24].

The two crosses in Fig. 3 represent the simulation performed by Kitsunezaki [22]. Whereas for $D=0.2$ his planar front was unstable, which is consistent with our analysis, his planar front for $D=1.0$ appeared to be stable, in apparent contradiction with our results. However, the simulations were done for a system of width $L_y=40$ and up to time $t=200$. From our results for the dispersion relation for $k=1$ and $D=1$ that is very similar to the one shown in Fig. 10 in Sec. III, we find that the characteristic length scale of the fastest growing mode is $L_m \approx 31$, while the associated characteristic time for this fastest growing mode is approximately $t_m = 520$. Hence, it is likely that the system width is too small and the simulation time too short to observe the instability. It would therefore be useful to redo the simulation for a bigger system and longer times. In fact, this illustrates the difficulty of using simulations alone to study systems, especially if only a few parameter values can be studied over a limited time range and system size. On the other hand, our explicit stability analysis allows us to map out the phase diagram in a relatively straightforward way.

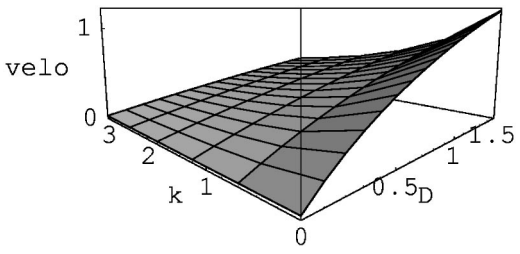

FIG. 1. The front velocity as a function of D and k, as determined from the analysis in Sec. II.

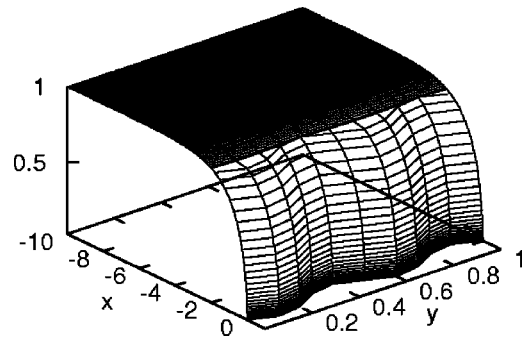

FIG. 2. Perturbed front profiles of bacteria densities. The front propagates into the x direction, and has a sinusoidal modulation in the y direction.

In Sec. IV we map the system with a moving boundary approximation to a sharp interface problem guided by the success this approach had in analyzing and understanding the Mullins-Sekerka instability mechanism [7], the long wave-

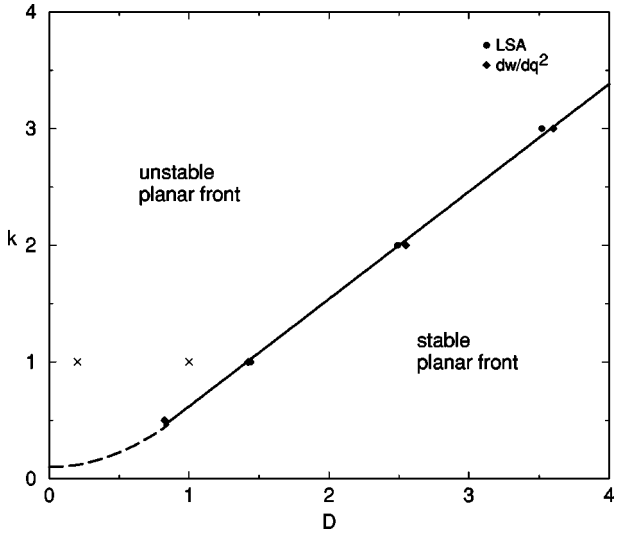

FIG. 3. Stability diagram for parameters D and k. Filled circles show where the region of stability of planar fronts starts as determined by a numerical linear stability analysis, filled diamonds show the same boundary as obtained from the solvability formula for $d^2\omega/dq^2|_{q=0}$ derived in Sec. III C. For $k=0.5$ both methods give the same value up to the size of the symbol. The solid line is there to guide the eye, the dashed line hints at the fact that while we expect the line of $D_c(k)$ to approach the origin we do not know the precise analytic behavior of $D_c(k)$ for $k \to 0$, since for $k=0$ the planar front is stable for all D [24,23]. The two crosses represent the simulation performed by Kitsunezaki [22]. For $D=0.2$ the front in these simulations was unstable, which is consistent with our analysis. For $D=1.0$ the planar front was stable, which does not agree with our analysis. The probable cause of this apparent discrepancy is discussed in the main text.

length instability associated very generally with diffusion-limited or Laplacian growth processes. We obtain by a multiscale expansion equations for b and n, which are valid in the outer bulk fields, and which are connected by boundary conditions. The boundary conditions are obtained by using solvability-type arguments to integrate out the internal degrees of freedom of the inner reaction region. As was already mentioned before, the moving boundary approximation is closest to the so-called one-sided growth models and is quite accurate for small D, but it never becomes mathematically correct in the limit $D\rightarrow 0$ for all dynamically relevant length scales.

II. PLANAR FRONT

There exist two trivial homogeneous solutions: The first is $n(x,t)=c_n, b(x,t)=0$, which implies some constant food level and no bacteria. This state is unstable since any amount of bacteria will be enough to let the bacteria density grow. The other trivial homogeneous state is $n(x,t)=0, b(x,t)=c_b$, which assumes a constant bacteria density and no food. This state is stable in the present model without sporulation. In addition there exist a steady-state solution in which the stable state $(c_b,0)$ propagates with a constant velocity v into the unstable state $(0,c_n)$, implying the propagation of the bacteria field into the nutrient field. Starting from an initial condition in which the unstable nutrient state is perturbed by a small amount of bacteria at the left, the bacteria field invades the nutrient state in the form of a well-defined reaction front propagating to the right. Since we are first interested in a planar front, we can restrict ourselves to one dimension. To obtain the uniformly translating front solution it is convenient to express the reaction-diffusion system in a comoving frame in which the new coordinate ξ travels with the velocity v_0 of the front, $\xi=x-v_0t$. The temporal derivative then transforms as $\partial_t|_x=\partial_t|_\xi-v_0\partial_\xi|_t$. For a front translating with uniform velocity v_0, the explicit time derivative vanishes and Eqs. (6),(7) reduce to

$$\frac{D}{k+1}\frac{d^2b^{k+1}}{d\xi^2}+v_0\frac{db}{d\xi}+nb=0, \tag{8}$$

$$\frac{d^2n}{d\xi^2}+v_0\frac{dn}{d\xi}-nb=0. \tag{9}$$

This is a system of two ODEs of second order. The boundary conditions at $\xi\rightarrow\pm\infty$ are given by the two homogeneous states. By choosing a right-moving front we obtain as boundary conditions at $\xi\rightarrow-\infty$ the stable state,

$$b(\xi\rightarrow-\infty)=c_b, \quad d_\xi b(\xi\rightarrow-\infty)=0, \tag{10}$$

$$n(\xi\rightarrow-\infty)=0, \quad d_\xi n(\xi\rightarrow-\infty)=0, \tag{11}$$

which invades the unstable state given at $\xi\rightarrow\infty$,

$$b(\xi\rightarrow\infty)=0, \quad d_\xi b(\xi\rightarrow\infty)=0, \tag{12}$$

$$n(\xi\rightarrow\infty)=c_n, \quad d_\xi n(\xi\rightarrow\infty)=0. \tag{13}$$

As mentioned before, the system simplifies extremely in the region where $b(\xi)=0$. By choosing the origin $\xi=0$ in such a way that for positive ξ $b(\xi)=0$, the system (8),(9) reduces in the positive ξ region to

$$b(\xi)=0, \tag{14}$$

$$\frac{d^2n}{d\xi^2}+v_0\frac{dn}{d\xi}=0, \tag{15}$$

which is a linear ODE for an n that can be solved analytically and is given by

$$n(\xi)=c_n-c_0\exp(-v_0\xi), \tag{16}$$

where $c_0>0$ is determined by the full problem. Hence, the system can be divided into two regimes, the first being $\xi>0$ given by Eqs. (14),(15) and can be solved analytically, and the second being $\xi<0$ that contains the full nonlinearity. Both regimes are connected via their common boundary conditions at $\xi=0$. Hence, it is sufficient to study Eqs. (8),(9) for $\xi<0$, for which we still have to determine the behavior at $\xi\rightarrow 0$ which we will obtain by studying the local behavior of the bacteria density b and the nutrient density n as ξ approaches zero from the left. Since the bacteria density b is a physical quantity, we assume it to be continuous. Moreover, Eq. (9) then implies that n and its derivative at the boundary have to be continuous as well. Hence, we obtain for n the boundary condition at $\xi=0$

$$n(0)=c_n-c_0, \tag{17}$$

$$\frac{dn}{d\xi}|_0=v_0c_0. \tag{18}$$

In the Introduction we have already discussed that the bacteria density b shows a singular behavior for $\xi\rightarrow 0$. This is due to the fact that the prefactor of the highest derivative in the b equation contains a factor b^k, which vanishes as $b\rightarrow 0$. This allows b to become singular near $\xi=0$. As is well known (see, e.g., [28]) at such a regular singular point one expects a behavior for b of the type [29]

$$b(\xi)=A(-\xi)^\alpha. \tag{19}$$

Substituting this ansatz into Eq. (8) we obtain

$$D\alpha[\alpha(k+1)-1]\ A^{k+1}(-\xi)^{\alpha(k+1)-2}-v_0A\alpha(-\xi)^{\alpha-1}-n_0A(-\xi)^\alpha=0. \tag{20}$$

To fulfill this equation the dominant terms in ξ, which are the first and second terms, have to be canceled. This determines A and α to be

$$A=\left(\frac{kv_0}{D}\right)^{1/k}, \tag{21}$$

$$\alpha=\frac{1}{k}. \tag{22}$$

Hence the bacteria density profile vanishes as

$$b(\xi)\to\left(-\frac{kv_0}{D}\xi\right)^{1/k} \quad \text{for} \quad \xi\to 0, \tag{23}$$

which implies that its derivative $db/d\xi$ diverges for $k>1$ as

$$\frac{db(\xi)}{d\xi}\to-\frac{A}{k}(-\xi)^{1/k-1} \quad \text{for} \quad \xi\to 0. \tag{24}$$

Hence, we are left to study Eqs. (8),(9) for $\xi<0$ with the boundary conditions (10), (11), (17), (23), and (24).

Due to the fact that we chose $f(n,b)=g(n,b)$, a conservation law is underlying the system (6),(7), expressing that all food is transformed into bacteria, i.e., that $c_b=c_n$. The conservation law allows us to reduce the order of our system of ODEs by one. Hence, by adding Eqs. (8) and (9) and integrating over space from $-\infty$ to ξ we obtain

$$\frac{D}{k+1}\frac{d^2b^{k+1}}{d\xi^2}+v_0\frac{db}{d\xi}+nb=0, \tag{25}$$

$$\frac{dn}{d\xi}+\frac{D}{k+1}\frac{db^{k+1}}{d\xi}+v_0b-v_0c_b=0. \tag{26}$$

Note that Eq. (26) immediately implies $c_b=c_n$ since the derivatives all vanish at $\xi\pm\infty$. This just expresses that food is converted into bacteria in this simplified model.

The one-dimensional front profile governed by Eqs. (8),(9) can be represented by a heteroclinic orbit in the $(b,d_\xi b,n)$ phase space connecting the two steady states corresponding to the boundary conditions (10)–(13). Due to the possibility of solving the system of ODEs analytically in the positive ξ region, the front profile can be found by applying a standard shooting method to the region $\xi<0$. By shooting from $\xi\to-\infty$ along the unstable manifold and requiring it to connect to the trajectory flowing into the singular origin with the boundary conditions (17), (23), and (24), a relationship between the velocity v_0 and the boundary condition $n(\xi=0)$ is uniquely selected. The existence of a unique front solution is also consistent with so-called counting arguments for the dimensions of the stable and unstable manifolds of the fixed points of the flow. On the left, for $\xi\to-\infty$, there is only one unstable mode leaving the homogeneous fixed point, which then fixes n and $d_\xi n$ at $\xi\to 0$ completely. Matching at $\xi=0$ to the positive ξ solution for n can only be done on a line in the $n-d_\xi n$ plane, since the n solution is an exponential. Hence, changing v_0 so as to match both fixes v_0 completely.

As we already anticipated at the end of Sec. I B, we henceforth choose $c_n=1$, and hence $c_b=1$: By appropriately rescaling ξ, v_0, and the n and b fields, any other choice for c_n can be transformed into the case with $c_n=1$ with renormalized diffusion coefficent $D_R=Dc_n^k$. The uniquely determined front velocity is hence essentially a function of D and k only,

$$v_0=v_0(D,k). \tag{27}$$

We shall now study the behavior of the front profiles and of $v_0(D,k)$ in more detail by a combination of observations from the numerical calculations and of simple analytical arguments. Many of these arguments can easily be formalized by asymptotic analysis or by reducing the equations in certain limits to simpler ones, but we shall refrain from doing so explicitly.

Figure 1 gives an idea of the functional dependence of the velocity v_0 on D and k. Figure 4 displays that for small D the velocity is linear in D,

$$v_0\approx a(k)D \quad (D\ll 1), \tag{28}$$

where $a(k)$ is a proportionality constant that decreases with increasing k.

This proportionality of v_0 with D for small D is simply a consequence of the fact that the propagation of the profile for small b is governed by the balance of the nonlinear diffusion with the $v_0db/d\xi$ term.

Figure 5 shows the dependence of the profile on D for $k=2$. With decreasing D the interfacial thickness W decreases, whereas the diffusion length of the nutrient density ℓ_n increases since

$$\ell_n=1/v_0, \tag{29}$$

as seen from Eq. (16). Hence, with decreasing D there is a separation of scales between the diffusion length ℓ_n and the interface width.

Figure 6 shows the dependence of the profile on k for fixed D, here $D=0.3$. It demonstrates that with increasing k the interfacial region decreases and sharpens.

At first sight, both Figs. 5 and 6 suggest that for small D or large k a moving boundary approximation might become appropriate. However, the behavior is rather subtle, and to prepare for a full discussion of this issue in Sec. IV, we analyze the scaling of the front profiles in some more detail.

To quantify the behavior of the interfacial thickness W as a function of k and D let us first measure the thickness at which the bacteria density reaches the level $b(W)=b_W=0.5$. Figure 7 shows how the interfacial thickness approaches a finite thickness as D approaches zero, and Fig. 8 shows how W approaches zero with increasing k. Both dependences can be understood by inverting Eq. (23),

$$W=\frac{D}{v_0k}b_W^k. \tag{30}$$

Since v_0 is proportional to D for small D, the interfacial thickness approaches a constant W_0:

$$W\to W_0=\frac{1}{a(k)k}b_W^k, \tag{31}$$

which depends only on k and the chosen interfacial value b_W. With increasing k, W_0 decreases, and vanishes for $k\to\infty$; indeed, for not too large values of b_W, we have

$$b^k\approx\exp(-k|\ln b_W|), \tag{32}$$

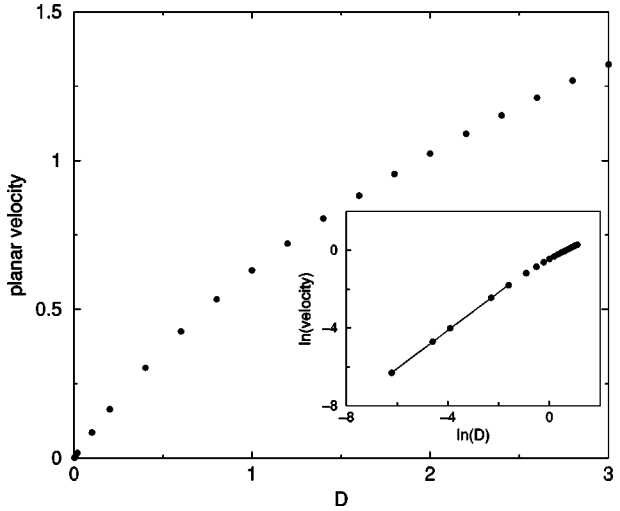

FIG. 4. Dependence of the planar velocity v_0 on D for $k=1$. The inset shows that for $D\to 0$ the velocity approaches zero linearly.

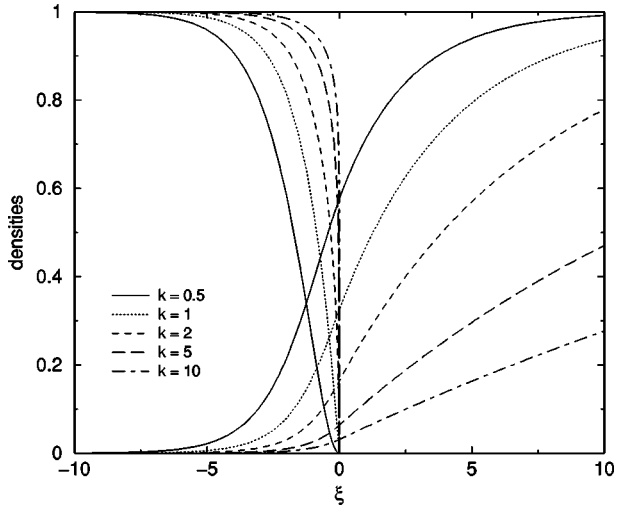

FIG. 6. Bacteria and nutrient density profiles for different k and fixed $D=0.3$.

so that W_0 vanishes exponentially. Note finally that Fig. 8 indicates that W becomes large as $k\to 0$; this indicates that the behavior of the model for $k\ll 1$ is quite different from that in the regime k of order 1 or larger, on which we will concentrate.

So far, we analyzed the width between the point where b reaches some fixed value $b_W<1$ and the point where b vanishes. In the limit $D\to 0$ this width remains finite, while for $k\to\infty$ the width measured this way vanishes. However, for addressing the question whether a sharp interface formulation can capture the essential behavior, it is also important to analyze how b approaches the asymptotic value 1 for large k. When k is large, we see that $n(\xi)$ becomes small in the interfacial zone. In fact, it is easy to convince oneself that the self-consistent scaling behavior of Eqs. (8),(9) for $\xi<0$ is $n(\xi)\sim 1/k$, $v_0\sim 1/k$ for large k, and this is born out by our numerical results (not shown). Furthermore, for v_0 small and $b\approx 1$, Eq. (9) for n reduces to $d^2n/d\xi^2-n=0$, showing that $n(\xi)$ decays to the left as $e^{-|\xi|}$. In other words, n decays into the bacterial zone on a length scale of order unity. Through the coupling term in Eq. (8), this also means that b decays to 1 towards the left on a scale of order unity—this is actually visible in Fig. 6. Thus, even though for large k b rises to values close to 1 on exponentially small length scales W, the scales over which b and n decay to their asymptotic values are actually of order unity.

III. LINEAR STABILITY ANALYSIS OF PLANAR FRONTS

A. Dispersion relation

To study the linear stability of the planar front, we have to perturb the front. Due to the singular behavior of the planar front the dynamically relevant perturbations are not just simply perturbations in the fields b and n but also in the shape of the singular line where $b\to 0$. Since we only study the linear

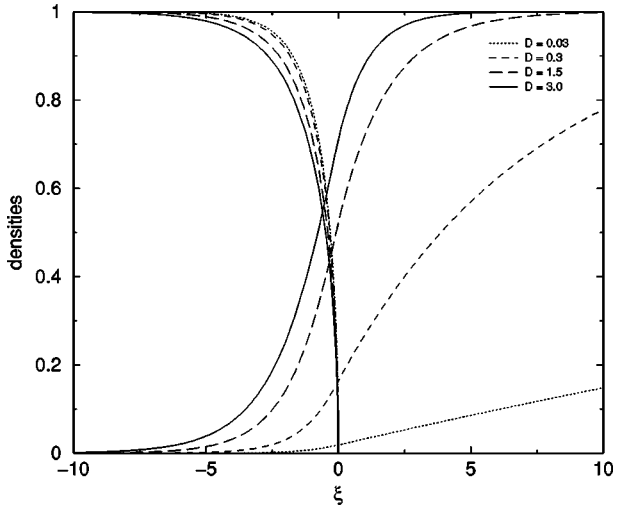

FIG. 5. Bacteria and nutrient density profiles for different D and fixed $k=2$.

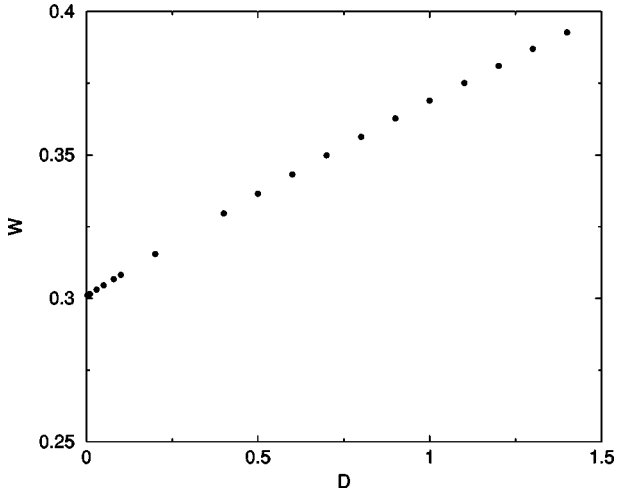

FIG. 7. Interfacial thickness as a function of D for fixed $k=2$. W is the distance from the origin to the point at which $b=0.5$.

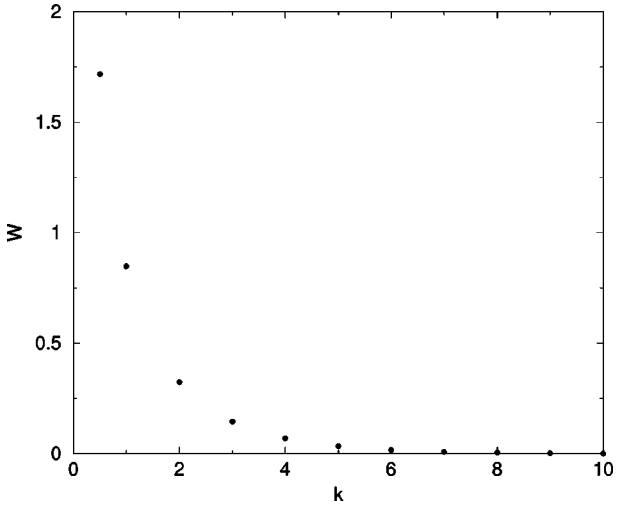

FIG. 8. Interfacial position as a function of k and for fixed $D=0.3$. W is the distance from the origin to the point at which $b=0.5$.

stability, we allow the perturbations to be complex and we can focus on a single mode with wave number q and amplitude ϵ by writing

$$h(y,t)=\epsilon\exp(iqy+\omega t).$$

We take this function h to be the modulation of the position of the line where the bacterial front vanishes, as indicated in Fig. 2. To be concrete, we now write b and n as

$$b(\xi,y,t)=b_0(\xi+h(y,t))+\epsilon b_1(\xi+h(y,t))\exp(iqy+\omega t), \tag{33}$$

$$n(\xi,y,t)=n_0(\xi+h(y,t))+\epsilon n_1(\xi+h(y,t))\exp(iqy+\omega t), \tag{34}$$

where (b_0,n_0) is the planar front solution determined in the previous section. This ansatz is the *crucial ingredient* that makes our stability analysis possible. The standard perturbation approach would amount to writing the perturbed field b as $b=b_0(\xi)+\epsilon b_1(\xi)e^{iqy+\omega t}$; such an ansatz works only if $b_0(\xi)$ is smooth enough that its derivative remains finite—here, because of the singular behavior of b_0, this standard approach fails. We therefore shift both the position of the singularity line of b_0 and of b_1, where b_1 and n_1 are the corrections to the bacterial profile and nutrition field as a result of this modulation. In order that perturbations are arbitrarily small as $\epsilon\to 0$ so that we can linearize the equations, we clearly need to have

$$\frac{n_1}{n_0}\ \text{bounded},\quad \frac{b_0}{b_1}\ \text{bounded}. \tag{35}$$

Moreover, of course, b_1 and n_1 should be continuous twice differentiable functions away from the singular line.

For the analysis, it will be convenient to introduce the locally comoving frame

$$\zeta=x-v_0t+h(y,t)=\xi+h(y,t)$$

in terms of which the fields can be written as

$$b(\zeta,y,t)=b_0(\zeta)+\epsilon b_1(\zeta)\exp(iqy+\omega t), \tag{36}$$

$$n(\zeta,y,t)=n_0(\zeta)+\epsilon n_1(\zeta)\exp(iqy+\omega t). \tag{37}$$

Upon linearization of the dynamical equations (6),(7) about the uniformly translating solution $(b_0(\xi),n_0(\xi))$, we then get

$$\mathcal{L}\begin{pmatrix} b_1\\ n_1\end{pmatrix}=\begin{pmatrix} \omega+\dfrac{D}{k+1}f'q^2 & 0\\ 0 & \omega+q^2\end{pmatrix}\begin{pmatrix} b_1+\dfrac{\partial b_0}{\partial\zeta}\\ n_1+\dfrac{\partial n_0}{\partial\zeta}\end{pmatrix}, \tag{38}$$

where $f=b_0^{k+1}$ and where the prime refers to a differentiation with respect to b_0. The terms proportional to $\partial b_0/\partial\zeta$ and $\partial n_0/\partial\zeta$ on the right result from the modulation h of the singular line about the line $\xi=0$ in the argument ζ of b_0 and n_0. Finally, the operator $\mathcal{L}$ is given by

$$\begin{aligned}\mathcal{L}_{11}&=\frac{D}{k+1}\frac{\partial^2}{\partial\zeta^2}(f')+v_0\frac{\partial}{\partial\zeta}+n_0\\ &=\frac{D}{k+1}f'\frac{\partial^2}{\partial\zeta^2}+\left(2\frac{D}{k+1}f''\frac{\partial b_0}{\partial\zeta}+v_0\right)\frac{\partial}{\partial\zeta}\\ &\quad+\frac{D}{k+1}f'''\left(\frac{\partial b_0}{\partial\zeta}\right)^2+\frac{D}{k+1}f''\frac{\partial^2 b_0}{\partial\zeta^2}+n_0,\end{aligned} \tag{39}$$

$$\mathcal{L}_{12}=b_0, \tag{40}$$

$$\mathcal{L}_{21}=-n_0, \tag{41}$$

$$\mathcal{L}_{22}=\frac{\partial^2}{\partial\zeta^2}+v_0\frac{\partial}{\partial\zeta}-b_0. \tag{42}$$

Note that the eigenvalue equation (38) is an ODE problem in terms of the variable ζ, in the same way as it is in the standard linear stability calculations [30].

Let us pause for a moment to reflect on the difference with the usual stability approach a bit more. Since the translational mode $(\partial_\zeta b_0,\partial_\zeta n_0)$ is the right zero eigenmode of $\mathcal{L}$,

$$\mathcal{L}\begin{pmatrix}\dfrac{\partial b_0}{\partial\zeta}\\ \dfrac{\partial n_0}{\partial\zeta}\end{pmatrix}=0, \tag{43}$$

we see that if we introduce

$$\overline{b_1}=b_1+\frac{\partial b_0}{\partial\zeta},\quad \overline{n_1}=n_1+\frac{\partial n_0}{\partial\zeta}, \tag{44}$$

in Eq. (38), then these new variables obey simply

$$\mathcal{L}\begin{pmatrix}\overline{b_1}\\ \overline{n_1}\end{pmatrix}=\begin{pmatrix}\omega+\dfrac{D}{k+1}f'q^2 & 0\\ 0 & \omega+q^2\end{pmatrix}\begin{pmatrix}\overline{b_1}\\ \overline{n_1}\end{pmatrix}. \tag{45}$$

This is precisely the linear equation one gets if one starts with the usual linear stability ansatz $b=b_0(\xi)+\overline{b_1}(\xi)\exp(iqy+\omega t)$, $n=n_0(\xi)+\overline{n_1}(\xi)\exp(iqy+\omega t)$ in terms of ξ rather than ζ as the variable. While at this level the two problems appear to be the same, their interpretation is not. When we write the perturbed problem in terms of the shifted coordinate ζ and require b_1/b_0 to remain bounded, then clearly Eq. (44) shows that the variable $\overline{b_1}$ is *more singular* than b_0—in particular, the singular behavior of $\overline{b_1}$ is that of $\partial b_0/\partial\zeta$. In other words, $\overline{b_1}/b_0$ is *not* a small perturbation, instead it diverges. Of course it is simply due to the fact that one cannot represent a shift of the singular line with a small perturbation in terms of fields that vanish at $\xi=0$. The ansatz we make in terms of the variable ζ, on the other hand, does represent a proper shift of this line; it can be thought of as a suitable resummation to capture this.

Let us return to the problem of solving for $b_1(\zeta)$ and $n_1(\zeta)$. Again we can split up the problem into two separate regions, since for $\zeta>0$ the problem simplifies to

$$b_1=0, \tag{46}$$

$$\frac{\partial^2 n_1}{\partial\zeta^2}+v_0\frac{\partial n_1}{\partial\zeta}-(\omega+q^2)n_1=(\omega+q^2)\frac{\partial n_0}{\partial\zeta}, \tag{47}$$

which is a linear ODE in n_1 that can be solved analytically,

$$n_1=(c_n-c_0)v_0\exp(-v_0\zeta)+d_0\exp(-\lambda\zeta), \tag{48}$$

with $\lambda=[v_0-\sqrt{v_0^2+4(\omega+q^2)}]/2$ and with d_0 being some constant that is undetermined at this stage [c_0 and c_n are parameters of the solution (16) for n_0]. This solution is connected to the negative ζ region via the boundary condition at $\zeta=0$ that determines d_0. To obtain the boundary condition at $\zeta=0$, we analyze the local behavior of b_1 and n_1 as $\zeta\to0$ from the left. Since n_1 and its derivative are continuous across $\zeta=0$, n_1 and $\partial_\zeta n_1$ obey at $\zeta=0$,

$$n_1=(c_n-c_0)v_0+d_0, \tag{49}$$

$$\partial_\zeta n_1=-(c_n-c_0)v_0^2-d_0\lambda. \tag{50}$$

In view of our requirement (35) that b_1/b_0 remains bounded, it is natural to assume that b_1 vanishes as

$$b_1=B(-\zeta)^\beta. \tag{51}$$

Indeed, by inserting it into Eq. (38) we straightforwardly obtain from the asymptotic behavior (19) for b_0,

$$B=-\frac{\omega A}{kv_0}=-\frac{\omega}{kv_0}\left(\frac{kv_0}{D}\right)^{1/k}, \tag{52}$$

$$\beta=\frac{1}{k}. \tag{53}$$

Hence, for $\zeta\to0$,

$$b_1(\zeta)=-\frac{\omega A}{kv_0}(-\zeta)^{1/k}=-\frac{\omega}{kv_0}b_0(\zeta), \tag{54}$$

so that

$$\frac{b_1(\zeta)}{b_0(\zeta)}\to\frac{\omega}{kv} \quad \text{for} \quad \xi\to0,$$

verifying that b_1/b_0 remains finite. Hence a solution b_1 that vanishes according to Eq. (51) does obey the requirement that perturbations are small everywhere. The boundary conditions at $\zeta\to-\infty$ are given by

$$b_1(\zeta)\to0, \quad \partial_\zeta b_1(\zeta)\to0, \tag{55}$$

$$n_1(\zeta)\to0, \quad \partial_\zeta n_1(\zeta)\to0, \tag{56}$$

since all perturbation should vanish at $\zeta\to-\infty$.

The linear dispersion relation is obtained by solving Eq. (38) for different q with the shooting method. By shooting from $\zeta\to-\infty$ along the unstable manifold and matching it to the trajectory leaving the origin with the boundary conditions (49), (50), and (54) we obtain a unique ω as a function of D, k, and q. At the same time d_0 is determined. Counting arguments for the multiplicity again support the uniqueness of ω. A numerical dispersion relation was obtained for $k=0.2,0.3,0.5,1,2,3$, and 5 and different D. For a fixed k the dependence of the dispersion relation on D is qualitatively the same for all k. Figure 9 shows the dispersion relation for $k=2$ and different D.

There is a long-wavelength instability for all $D<D_c(k)$, whereas all modes are stable for $D>D_c(k)$. As D decreases below D_c the growth rate of the unstable modes starts to increase as does the range of wave numbers that are unstable. At the same time both q_m, the wave number that corresponds to the maximum growth rate, as well as q_c, the wave number for which $\omega=0$, shift with decreasing D to larger wave numbers. By decreasing D even further we observe that the growth rate starts to decrease again, which is due to the fact that the whole dynamics of the front is slowing down as we decrease D. Note, however, that as D becomes small, the range of unstable wave numbers does not vary appreciably: q_c is roughly constant.

The dependence of the dispersion relation on k is shown in Fig. 10. We know that for $k=0$ the planar front is stable. For small k the front starts to be unstable for long-wavelength perturbations. With increasing k the range of unstable modes is increasing as is the growth rate. However, at $k>1$ the growth rate starts to decrease again which is again, due to the fact that the whole dynamics of the front slows down as k is increasing. q_m shows qualitatively the same behavior as q_c. It starts to shift with increasing k to a shorter wave length, stays constant for $k=0.5$ to $k=3$, and then decreases again to a longer wave length. Figure 3 shows how

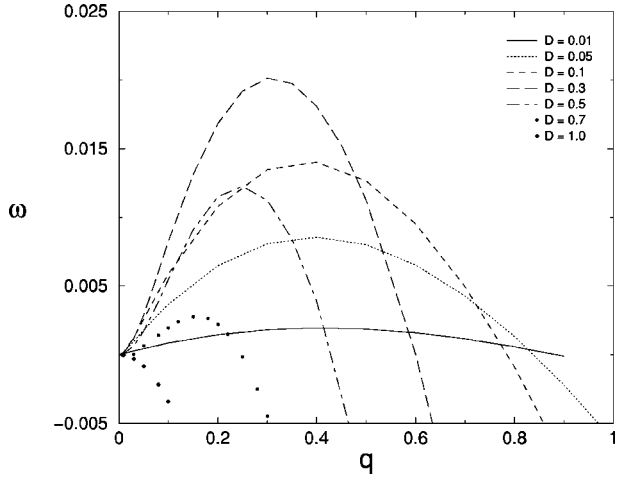

FIG. 9. Dispersion relation for $k=2$ and different D. For $D<D_c$ the planar front is unstable for $q<q_c$ whereas for $D>D_c$ it is linearly stable for all q.

D_c depends on k. With increasing k, the transition value D_c increases, thus implying that with increasing k the region of instability is larger. For large k the value of $D_c(k)$ appears to be linear in k.

One general noteworthy feature of our results is that the growth rate of the most unstable mode as well as the corresponding wave number q_m are generally rather small. As we have discussed already in Sec. I, this may the reason that Kitsunezaki [22] appears to observe a planar stable interface in the region of the phase diagram where planar interfaces are unstable according to our calculation.

B. Comparison with the Mullins-Sekerka instability

The dispersion relation of the planar bacterial fronts is, for $D<D_c(k)$ and away from the instability line $D_c(k)$, similar to the so-called Mullins-Sekerka dispersion relation

$$\omega_{MS}=v_0|q|(1-d_0\ell_{th}q^2) \tag{57}$$

such that one derives for perturbations of a planar crystallization interface [7]. In this case, $\ell_{th}=D_{th}/v_0$ is the thermal

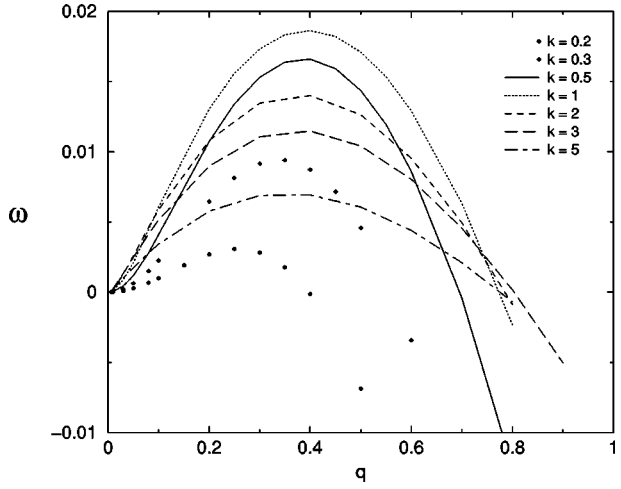

FIG. 10. Dispersion relation for $D=0.3$ and different k.

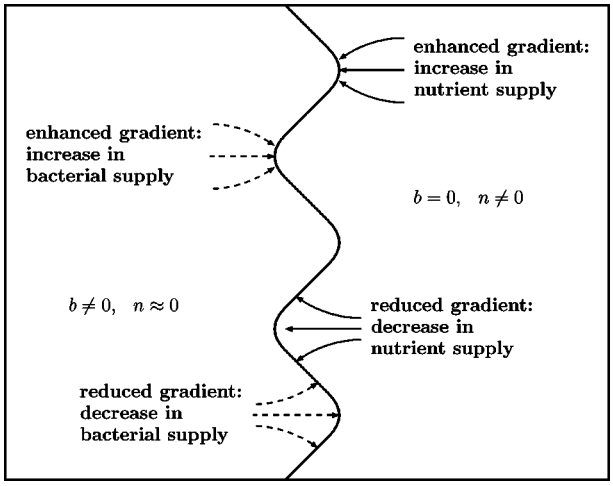

FIG. 11. Sketch of a perturbed front propagating from the left to the right. The arrows drawn with a full line indicate the diffusion flow of nutrient, on the front side of the interface, those drawn with a dashed line the diffusion current of bacteria. At a protrusion into the nutrient region, the nutrient diffusion is enhanced while the bacterial diffusion current is suppressed. There are hence two competing effects, whose relative strength depends on D.

diffusion length (the analog of our nutrient diffusion length ℓ_n), and d_0 is a microscopic surface-tension-like length that measures the strength of the curvature corrections to the interface. We shall see later in Sec. IV why this analogy is justified, but it already shows us here something interesting: As $D\to 0$, v_0 vanishes proportional to D. In this limit ℓ_{th} diverges just like ℓ_n does. Hence, from the observation that the range of unstable modes remains finite in this limit, and hence that the term analogous to $d_0\ell_{th}$ remains finite, we can immediately conclude that the ''effective surface tension'' of our bacterial fronts, the analog of d_0 in Eq. (57), should scale as D for small D.

That a propagating, planar reaction-diffusion front shows a long-wavelength instability for small D but is linearly stable for all q for $D>D_c$, has been observed and explained before (see, e.g., [24]), and can be understood in the following way. Let us consider a perturbed front moving to the right as sketched in Fig. 11. At a protrusion into the nutrient side of the interface, the nutrient gradients are compressed and hence the nutrient diffusion is enhanced. The ''feeding'' of the interface from the nutrient side is hence enhanced there, and this tends to make such protrusions grow larger in time. On the other hand, as the dashed arrows indicate, the bacterial diffusion flow from the back side towards the interface is reduced at such a protrusion—this tends to reduce the growth of such protrusions, and hence to stabilize the interfacial perturbation. The relative strength of the two effects is determined by D, the effective diffusion constant of the bacteria behind the interface. When $D>D_c(k)$, the stabilizing effect from the backside wins, for $D<D_c(k)$ the destabilizing effect on the front side dominates. Even the effect on k can be understood in this context. The effective diffusion coefficient is given by $D=Db^k$, which lowers the effective diffusion coefficient in the interfacial region where $b<1$. Hence, the bigger the k the smaller the effective diffusion

constant in the interfacial region, the longer the destabilizing effect of the nutrient can prevail. When k decreases towards zero, the stabilizing bacterial diffusion extends more and more towards the front region [31].

As we have pointed out above, in the limit $D \ll D_c(k)$ the instability is very much like the classical Mullins-Sekerka instability of a crystal-melt interface. As D increases towards D_c this connection breaks down because the stabilizing diffusion from the backside becomes important *within* the interfacial zone: There is then no clear separation anymore between an interface and the regions before and behind the front [see also Sec. IV C for further discussion of the behavior for D near $D_c(k)$].

Of course, the competition between the stabilizing effect of the diffusion gradient on the backside and the destabilizing effect of the gradient on the front of the interface shows up in crystal growth during transient regimes and can be understood along the lines of the Mullins-Sekerka stability analysis [7]. A most amusing and dramatic illustration of this was observed recently in experiments on the melting of polarized ^{3}He [32]; there the instability sets in only after a very long transient because the diffusion coefficient on the backside is very much bigger than on the front; as a result, as long as there is a transient gradient on the backside, the melting interface remains stable.

C. Onset of instability

As we have found above that the instability that occurs when D decreases below $D_c(k)$ is a long-wavelength $q=0$ instability, the critical line $D=D_c(k)$ is the line where $d\omega/d(q)^2|_{q=0}=0$: to the right of this line in Fig. 3 this derivative is negative and to the left of it it is positive, so that $\omega>0$ for small q. Since the translational mode $q=0$ is the eigenmode of $\mathcal{L}$ with eigenvalue $\omega=0$, we can investigate the behavior of the ω-q^2 curve in the vicinity of the origin by the following expansion [25]. Because the $q=0$ mode is a translation mode with zero eigenvalue, ω is small and of order q^2 when q is small. Moreover, $b_1=0$ and $n_1=0$ for $q=0$, and so for small q, b_1, and n_1 are both of order q^2 too. In Eq. (38) this implies that for q small, the terms on the right-hand side involving b_1 and n_1 are of order q^4. To order q^2, we therefore get

$$\mathcal{L}\begin{pmatrix} b_1 \\ n_1 \end{pmatrix} = \begin{pmatrix} \omega + \dfrac{D}{k+1} f' q^2 & 0 \\ 0 & \omega + q^2 \end{pmatrix} \begin{pmatrix} \dfrac{\partial b_0}{\partial \zeta} \\ \dfrac{\partial n_0}{\partial \zeta} \end{pmatrix}, \quad (58)$$

which is exact to order q^2. Since $\mathcal{L}$ has a zero eigenvalue, we can apply the solvability condition by requiring that the inner product with the left zero mode of $\mathcal{L}$ vanishes,

$$\int_{-\infty}^{\infty} d\zeta \begin{pmatrix} \Psi_1 \\ \Psi_2 \end{pmatrix}^T \begin{pmatrix} \omega + \dfrac{D}{k+1} f' q^2 & 0 \\ 0 & \omega + q^2 \end{pmatrix} \begin{pmatrix} \dfrac{\partial b_0}{\partial \zeta} \\ \dfrac{\partial n_0}{\partial \zeta} \end{pmatrix} = 0. \quad (59)$$

Here Ψ_1 and Ψ_2 are the components of the left zero mode, i.e., of the right zero eigenvector of the adjoint matrix operator $\mathcal{L}^*$,

$$\mathcal{L}^* = \begin{pmatrix} \dfrac{D}{k+1} f' \dfrac{\partial^2}{\partial \zeta^2} - v_0 \dfrac{\partial}{\partial \zeta} + n_0 & -n_0 \\ b_0 & \dfrac{\partial^2}{\partial \zeta^2} - v_0 \dfrac{\partial}{\partial \zeta} - b_0 \end{pmatrix}. \quad (60)$$

Upon rewriting Eq. (59) as

$$\omega \int_{-\infty}^{\infty} d\zeta \left(\Psi_1 \frac{\partial b_0}{\partial \zeta} + \Psi_2 \frac{\partial n_0}{\partial \zeta} \right) = -q^2 \int_{-\infty}^{\infty} d\zeta \left(\frac{D}{k+1} \Psi_1 f' \frac{\partial b_0}{\partial \zeta} + \Psi_2 \frac{\partial n_0}{\partial \zeta} \right), \quad (61)$$

and taking the limit $q^2 \to 0$, this leads to the required exact relation for the onset of the lateral instability,

$$\left. \frac{d\omega}{d(q^2)} \right|_{q=0} = - \frac{\displaystyle\int_{-\infty}^{\infty} d\zeta \left(\frac{D}{k+1} \Psi_1 f' \frac{\partial b_0}{\partial \zeta} + \Psi_2 \frac{\partial n_0}{\partial \zeta} \right)}{\displaystyle\int_{-\infty}^{\infty} d\zeta \left(\Psi_1 \frac{\partial b_0}{\partial \zeta} + \Psi_2 \frac{\partial n_0}{\partial \zeta} \right)}. \quad (62)$$

Planar fronts change stability when the integral in the numerator of Eq. (62) changes sign.

Since $\mathcal{L}$ is non-Hermitian, there is no obvious relationship between the zero right eigenmode of $\mathcal{L}$ and its adjoint $\mathcal{L}^*$. To find the zero right eigenvector of the adjoint operator $\mathcal{L}^*$ we have to impose appropriate boundary conditions on the left eigenmodes too. Generally, the boundary conditions of the functions in the left adjoint space are obtained from the definition of the adjoint operator, in that for all functions Φ we consider we need to have

$$\int_{-\infty}^{\infty} d\zeta \Psi (\mathcal{L}\Phi) = \int_{-\infty}^{\infty} d\zeta (\mathcal{L}^* \Psi) \Phi. \quad (63)$$

In general, when the partial integrations are done so as to obtain $\mathcal{L}^*$ from $\mathcal{L}$, we obtain boundary terms; the requirement that these vanish give the boundary conditions on the adjoint functions Ψ. In the present case, since the functions on which our operators are working are defined on the infinite interval $(-\infty,\infty)$ for n_1 and its related left component Ψ_2, and on the semi-infinite interval $(-\infty,0]$ for b_1 and Ψ_1, we find that the appropriate boundary condition for the adjoint functions Ψ is that Ψ_2 should stay bounded as $\pm\infty$; likewise Ψ_1 should stay bounded both as $\zeta \to -\infty$ and as $\zeta \to 0$.

We are now in a position to analyze the behavior of the adjoint eigenmodes; we will report the analysis in some de-

tail, as the various elements form important ingredients of the derivation of a moving boundary approximation in the following section. $\mathcal{L}^*$ simplifies again considerably in the positive ζ region due to the fact that b_0 vanishes identically there, so it is again of advantage to split the region of integration into two, $\zeta<0$ with $\mathcal{L}^*$ given by Eq. (60), and $\zeta>0$ for which

$$\mathcal{L}^*=\begin{pmatrix} -v_0\dfrac{\partial}{\partial\zeta}+n_0 & -n_0 \\ 0 & \dfrac{\partial^2}{\partial\zeta^2}-v_0\dfrac{\partial}{\partial\zeta} \end{pmatrix}. \tag{64}$$

For $\zeta>0$ Ψ_2 has to solve the homogeneous ODE

$$\frac{\partial^2\Psi_2}{\partial\zeta^2}-v_0\frac{\partial\Psi_2}{\partial\zeta}=0. \tag{65}$$

This equation has two independent solutions, a constant and an exponential that diverges for increasing ζ. Hence the boundary condition that Ψ_2 remains bounded immediately gives the solution

$$\Psi_2=\psi_0=\text{const}, \quad \zeta>0. \tag{66}$$

Moreover, the differential equations for Ψ_2 implied by the zero-eigenvalue equation

$$\mathcal{L}^*\begin{pmatrix}\Psi_1\\ \Psi_2\end{pmatrix}=0 \tag{67}$$

shows that Ψ_2 has to be continuous and has to have a continuous derivative at $\zeta=0$. Hence, when we construct the eigenmodes on the left half space $\zeta<0$, the Ψ_2 component has to obey the boundary conditions

$$\Psi_2(\zeta=0)=\psi_0, \qquad \partial\Psi_2/\partial\zeta|_{\zeta=0}=0. \tag{68}$$

Since b_0 vanishes identically for $\zeta>0$, we need to know Ψ_1 only in the region $\zeta<0$. As we stated above, because the functions b_1 that we consider all vanish as $\zeta\uparrow 0$, the definition of the adjoint operator does not imply a boundary condition on $\Psi_1(\zeta=0)$ as long as it does not diverge. A straightforward analytical investigation of the equation near $\zeta=0$ shows that in general Ψ_1 will, with a finite slope, approach a finite value as $\zeta\uparrow 0$, and that in general it has a higher-order singular term $\sim(-\zeta)^{(1+D/k)}$.

We now turn to the behavior as $\zeta\to-\infty$. In this limit, $n_0\to 0$ and $b_0\to 1$, so $\mathcal{L}^*$ reduced from Eq. (60) to

$$\mathcal{L}^*=\begin{pmatrix} D\dfrac{\partial^2}{\partial\zeta^2}-v_0\dfrac{\partial}{\partial\zeta} & 0 \\ 1 & \dfrac{\partial^2}{\partial\zeta^2}-v_0\dfrac{\partial}{\partial\zeta}-1 \end{pmatrix}. \tag{69}$$

It is easy to verify that as $\zeta\to-\infty$, there are three possible types of nondivergent zero mode solutions,

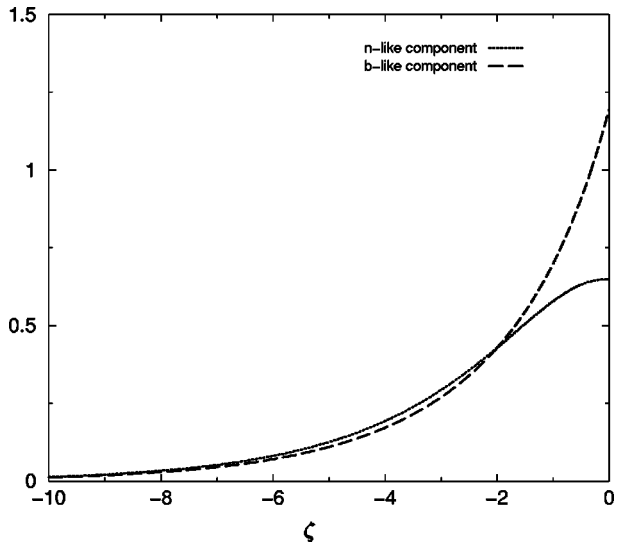

FIG. 12. Zero right eigenvector $\overline{\Psi}^{(2)}$ of the adjoint operator $\mathcal{L}^*$ for $k=2$ and $D=0.3$. The *b*-like component Ψ_1 approaches a finite value at $\zeta=0$ with a finite slope; it generally has a higher-order singular term $\sim(-\zeta)^{(1+D/k)}$.

$$\Psi^{(1)}\sim\begin{pmatrix}1\\1\end{pmatrix}, \qquad \Psi^{(2)}\sim e^{v_0\zeta/D}, \qquad \Psi^{(3)}\sim e^{\lambda_+\zeta}. \tag{70}$$

Here $\lambda_\pm=(v_0\pm\sqrt{v_0^2+4})/2$, so that the mode $\sim e^{\lambda_+\zeta}$ indeed converges towards the left; the other mode allowed by the linear equations, $e^{\lambda_-\zeta}$, on the other hand, diverges towards the left, and hence is forbidden by the boundary conditions.

The mode $\Psi^{(1)}$ is very special—it is immediately verified from Eq. (60) that

$$\mathcal{L}^*\begin{pmatrix}\psi_0\\ \psi_0\end{pmatrix}=0 \quad \text{for all } \zeta \ (\psi_0 \ \text{const}), \tag{71}$$

not just for $\zeta\to-\infty$. In other words, the constant mode $\Psi^{(1)}$ is an exact adjoint zero mode for all $\zeta\leqslant 0$.

If we integrate $\Psi^{(2)}$ or $\Psi^{(3)}$ forward towards increasing ζ, each trajectory in the phase space of the ODE is uniquely determined (apart from an overall amplitude, as the equations are linear). Hence, if we follow either $\Psi^{(2)}$ or $\Psi^{(3)}$ towards $\zeta=0$, the derivatives $\partial_\zeta\Psi^{(2)}|_{\zeta=0}$ and $\partial_\zeta\Psi^{(3)}|_{\zeta=0}$ will in general be *nonzero*. As we have, however, seen above, in order that the full eigenmodes on the whole real axis remain bounded also for $\zeta\to\infty$, the Ψ_2 component needs to have a zero derivative at $\zeta=0$ [see Eq. (68)]. Each separate eigenmode does not obey this requirement, but by the linearity of the equation it will always be possible to construct one unique linear combination $\overline{\Psi}^{(2)}$ of $\Psi^{(2)}$ and $\Psi^{(3)}$ that does have zero derivative. This solution constitutes the second adjoint zero eigenmode of the problem. Like the trivial eigenmode $\Psi^{(1)}$, it can be extended smoothly to the required $\overline{\Psi}_2^{(2)}=\text{const.}$ behavior for $\zeta>0$.

Figure 12 shows the adjoint zero eigenmode $\overline{\Psi}^{(2)}$ of $\mathcal{L}^*$ for $k=2$ and $D=0.3$, obtained numerically from the ODEs with a shooting method. The qualitative behavior of the com-

ponents is in agreement with the above discussion, and is independent of the values of the parameters. Note that the b-like component $\overline{\Psi}_1^{(2)}$ approaches a finite value at $\zeta=0$ with a finite slope; this behavior is also found for arbitrary parameters, while as is easily verified there generally is a parameter-dependent subdominant singular term proportional to $|\zeta|^{(1+D/k)}$.

To obtain the onset of lateral instability the adjoint zero eigenmode has to be convoluted with the translational mode $(\partial_\zeta b_0, \partial_\zeta n_0)$ according to Eq. (62). Which of the two zero modes should we use? The trivial adjoint zero mode $\Psi^{(1)}$ expresses change of velocity under reparametrization, and is related to conservation law in our system [see the discussion after Eq. (26)]; this will become more clear in the following section. It does not play a role for the onset of instability; we will therefore ignore it here [33] and use $\overline{\Psi}^{(2)}$ to evaluate Eq. (62). A change of sign of the numerator, which marks the onset of instability, is obtained for $k=0.5$, 1, 2, and 3 and shown in Fig. 3 as diamonds. In the figure, these values are also compared to the D_c determined by the numerical dispersion relation shown in Fig. 3 as filled dots. The agreement is very good, as it should; we have also checked that away from this line, a fit of the small-q behavior of the dispersion relation leads to values of the second derivative of ω at $q=0$, which are consistent with the solvability formula. These results thus confirm the consistency of our full stability calculation and the solvability expression for the critical line in the phase diagram and the small q behavior of the growth rate ω.

IV. SHARP INTERFACE FORMULATION

A moving boundary approximation or sharp interface formulation is appropriate when the width of the front or interface is much smaller than the typical length scale of the pattern and when the dynamics of the pattern occurs through the motion of these interfaces. The moving-boundary approximation amounts then to treating these fronts as mathematically sharp interfaces or boundaries by taking their width to zero and integrating out their internal degrees of freedom. There are three important assumptions underlying such an approximation, namely, (a) that there is a separation of length scales, (b) that there is a separation of time scales between the motion of the front as a whole and its internal dynamics, and (c) that the internal dynamics of the front is determined by the nonlinear front region itself, so that the solvability-type integrals are dominated by the contributions from the finite region, and hence do not diverge. The latter condition is violated in practice only for special types of fronts propagating into a linearly unstable state, so-called ''pulled'' fronts [34,35]; our fronts are not of this type (they are of the ''pushed'' type, in this terminology), so we focus our analysis on the length and time scale requirements (a) and (b).

As we saw in Sec. III, the planar front width is finite, even for $D\to 0$ at fixed k. Moreover, even though for $k\to\infty$ the b field rises over an exponentially small distance behind the singularity line, both the b and n fields even then, only approach their asymptotic values over a distance of order unity. In this sense, even in this limit the front width W remains finite. Of course, we can always *choose* to investigate fronts whose curvature κ is small in the sense that $\kappa W\ll 1$. For these, a moving boundary approximation should be accurate; we do find, indeed, below that the sharp interface formulation we derive for the present problem is consistent with the result of the dispersion relation of Sec. III for q small enough that $qW\ll 1$. However, whether such a moving boundary approximation applies *at all dynamically relevant length scales*, is another matter. We already know from the analysis of the dispersion relation in Sec. III that in the left part of the D-k-phase diagram modes up to $q=q_c$ are unstable, and that q_c is generally finite, except close to the critical line $D=D_c(k)$. Hence, q_cW remains finite as well, and so there is no obvious limit where a moving boundary approximation becomes asymptotically correct on all dynamically relevant length scales. Nevertheless, we find that in practice the sharp interface formulation that we develop is rather accurate in a significant portion of the phase diagram. Since the present problem has some unusual and new aspects, we focus again on the essential structure and intuitive arguments, rather than mathematical rigor.

A. Sharp interface formulation of the problem

The simplest case to consider to guide our intuition is the limit $D\ll 1$. As we discussed in connection with Fig. 5, in this regime the bacterial density field approaches its asymptotic value on the finite scale W, while the n-diffusion field in front of the bacterial front decays on a length scales $l_n=1/v_0$, which diverges as $D\to 0$ since $v_0\sim D$. A sharp interface formulation is then based on the idea that we view the bacterial front on the ''outer'' scale ℓ_{out} on which the patterns and diffusion fields vary in the presence of the moving boudary, which is treated as a sharp line of zero thickness. The dynamics of the fields on the ''inner'' scale [36,37] of the front (W), and the way in which this dynamics responds to changes in the fields on both sides of this inner zone, is translated into boundary conditions for the outer fields in the interfacial formulation. Formally, the moving boundary consists of taking the limit $\delta\equiv W/\ell_{out}\to 0$.

Normally, a sharp interface formulation or moving boundary approximation is based on applying the theory of matched asymptotic expansions [28,37]. Here, the situation is somewhat unusual: on the right side of the inner region (the interfacial transition zone where essentially the nutrient is consumed by the bacteria) we already have a sharply defined boundary, the singular line where b vanishes. At this side, we therefore do not have a matching problem, instead we already have two boundary conditions for the n field, namely, the requirements that the value of n and the gradient of n are continuous at the singular line where b vanishes—this follows directly from the dynamical equation (7), since the ''reaction term'' $-nb$ is continuous. On the left side of the interfacial zone, on the other hand, the b field varies continuously and we do have a true matching problem.

In our present case, the ''outer field'' on the front side of the interface is simply the n field in the whole region to the right of the singular line where b vanishes; hence there the

nutrient field n obeys a simple linear diffusion equation,

$$\text{front side ``outer'' Eqs.:} \begin{cases} b=0, \\ \dfrac{\partial n}{\partial t}=\nabla^2 n. \end{cases} \tag{72}$$

It is useful to introduce a suitable curvilinear coordinate system in which $\xi=0$ coincides with the singular line where b vanishes. In the sharp interface limit, the line $\xi=0$ then also coincides with the position of the moving interface. We furthermore identify the region ahead of the front as the $+$ side of the interface where $\xi>0$, and use a superscript $+$ to indicate values of the outer field extrapolated from the outer region towards the line $\xi=0$: $n^+=\lim_{\xi\downarrow 0} n(\xi)$, $\nabla n^+ = \lim_{\xi\downarrow 0}\nabla n(\xi)$. As we have already mentioned, n and its gradient should be continuous at this line, and we can therefore write the boundary conditions as

$$\lim_{\xi\uparrow 0} n(\xi)=n^+, \quad \lim_{\xi\uparrow 0}\nabla n(\xi)=\nabla n^+. \tag{73}$$

We now turn to the behavior on the backside of the front, the $-$ side. We have seen that in the bacterial front, the nutrition field decays exponentially fast to zero towards the left on a length scale of order unity; hence, in the $-$ outer region behind this interfacial zone, we have $n\approx 0$ for the nutrition field. The bacterial field is close to 1 there. Therefore, we take the dynamics of the b-field into account there, by writing $b=1+\Delta b$ and linearizing in the outer field Δb,

$$\text{back side ``outer'' Eqs.:} \begin{cases} \dfrac{\partial \Delta b}{\partial t}=D\nabla^2 \ \ \Delta b, \\ n=0. \end{cases} \tag{74}$$

Note that the outer equations (72) and (74) have been written in the laboratory frame, not in a comoving frame, since in the case of nontrivial patterns, there is no single relevant comoving frame.

What are the boundary conditions on the $-$ side of the front? According to the matching prescription, *the inner field expanded in the outer variables on the back side should equal the outer field expanded in the inner variables* [37]. Extrapolating the inner field in the outer variables towards the $-$ side means that we investigate the b profile to the left towards $-\infty$. As Figs. 5 and 6 illustrate, on the inner scale W the b field rapidly approaches a constant value. Although these figures are made for planar fronts, the analysis below shows that this continues to hold for weakly curved fronts and that the appropriate matching conditions are

$$\text{matching condition:} \begin{cases} \lim\limits_{\xi\to-\infty} b(\xi)=1+\Delta b^-, \\ \lim\limits_{\xi\to-\infty} \nabla b(\xi)=0. \end{cases} \tag{75}$$

Here Δb^- is the value of the outer field Δb extrapolated from the outer $-$ region towards the interface. Note that the second condition that the gradient vanishes, is also consistent with the matching prescription: if we assume that the outer field Δb varies on the outer scale $\mathbf{X}=\delta\mathbf{r}$ with $\delta=W/\ell_{out}$ then the outer gradient of Δb rewritten in terms of the inner variable vanishes in the limit $\delta\to 0$.

Now that we know how to connect the inner fields to the outer ones—on the left side of the inner region through the matching conditions (75), on the right side through boundary conditions (73)—we are ready to derive the effective boundary conditions in a sharp-interface formulation. One easily gets convinced that in order to get a well-posed moving boundary problem with the above outer dynamical equations and matching conditions, one needs effectively *three* boundary conditions relating Δb^-, n^+, and ∇n^+ and the interface velocity and curvature. To derive them, we imagine that the front is weakly curved with curvature κ such that $\kappa W\propto\delta \ll 1$. Since we identified the line $\xi=0$ with the line where b vanishes, ξ is a local comoving coordinate with speed v in the direction perpendicular to the front. In this weakly curved system, we then have on the inner scale

$$\frac{\partial b}{\partial t}=\frac{D}{k+1}\frac{\partial^2 b^{k+1}}{\partial \xi^2}+(v+D\kappa\, b^k)\frac{\partial b}{\partial \xi}+nb, \tag{76}$$

$$\frac{\partial n}{\partial t}=\frac{\partial^2 n}{\partial \xi^2}+(v+\kappa)\frac{\partial n}{\partial \xi}-nb. \tag{77}$$

Following standard practice, we now ignore the time derivatives on the left (taken in the comoving frame). This amounts to an adiabaticity assumption, that the change in the pattern and hence in the front speed and profile, taking place on time scales much longer than the relaxation time of the front [assumption (b) discussed in Sec. IV A above]. Technically, it means that the solution stays always close to a uniformly translating solution in the curved coordinate system, and our goal now is to calculate the changes in the velocity perturbatively. Indeed, let us write $v=v_0+v_1$, where v_0 is the velocity of the planer solution and v_1 the change in velocity due to the curvature and the fact that the outer field n is changed slightly from the planar solution; similarly, we write $b=b_0+b_1'$ and $n=n_0+n_1'$ so that b_1' and n_1' are the deviations in the fields from the planer solutions (we use the prime to emphasize the difference from the perturbations used in the linear stability analysis). Upon linearization about the planar front solution, we then get the equation

$$\mathcal{L}\begin{pmatrix} b_1' \\ n_1' \end{pmatrix}=\begin{pmatrix} -v_1-D\kappa\, b_0^k & 0 \\ 0 & -v_1-\kappa \end{pmatrix}\begin{pmatrix} \dfrac{\partial b_0}{\partial \xi} \\ \dfrac{\partial n_0}{\partial \xi} \end{pmatrix}, \tag{78}$$

where $\mathcal{L}$ is the same operator introduced before in Eq. (38), written now in terms of the variable ξ. This equation again calls for applying the solvability condition. We have already seen in Sec. III C that the operator $\mathcal{L}$ has a number of adjoint zero eigenmodes. There is a subtle difference between the present analysis and the one of Sec. III C, however, which is

crucial for obtaining the proper boundary conditions. In the stability analysis of Sec. III C we worked with functions defined on the whole interval $(-\infty,\infty)$; this implied that the mode constructed for negative ζ needed to have zero derivative of the Ψ_2 component at $\zeta=0$ [38], and this reduced the number of proper adjoint zero eigenmodes to two. Here, however, we are doing perturbation analysis only in the inner region, which in the inner variable is the semi-infinite interval $(-\infty,0]$. We, therefore, do not require now the adjoint zero mode to have $\partial\Psi_2/\partial\xi|_{\xi=0}=0$, and hence we now have *three* rather than two admissible adjoint zero modes. These lead to the three necessary equations that become the boundary conditions sought for in the sharp interface formulation. Moreover, because we now work on a semi-infinite interval, we get boundary terms at $\xi=0$ from the partial integrations necessary to have the operator work on the adjoint functions [39],

$$\begin{aligned}\int_{-\infty}^{0} d\xi\ \ (\Psi_1,\Psi_2)\mathcal{L}\begin{pmatrix} b_1' \\ n_1' \end{pmatrix} &= \int_{-\infty}^{0} d\xi\left[\mathcal{L}^*\begin{pmatrix}\Psi_1\\ \Psi_2\end{pmatrix}\right]^T\begin{pmatrix} b_1' \\ n_1' \end{pmatrix} \\ &\quad -\Psi_1(-\infty)\,v_0\Delta b^- - \frac{\partial\Psi_2}{\partial\xi}\Big|_{\xi=0}(n^+-n_0^+) \\ &\quad +\Psi_2(0)[\nabla_\xi n^+ - \nabla_\xi n_0^+ + v_0(n^+-n_0^+)]. \end{aligned} \tag{79}$$

Here we have used the boundary and matching conditions (75) and (73) for the deviations b_1' and n_1' from the planar values b_0 and n_0. Note that there are no boundary terms in the field b_1' at $\xi=0$, since these are all proportional to b_0^k, and $b_0^k(\xi\to 0)$ vanishes according to Eq. (23).

The three boundary conditions now straightforwardly follow by taking the left inner product of the three zero modes with Eq. (78) together with Eq. (79). The behavior of the three adjoint zero modes of $\mathcal{L}^*$ on the left for $\xi\leqslant 0$ has been discussed already in Sec. III C. The first one is simply $\Psi_1^{(1)}=\Psi_2^{(1)}=\text{const}$. In this case we immediately obtain

$$\begin{aligned} -v_0\Delta b^- + (\nabla_\xi n^+ - \nabla_\xi n_0^+) + v_0(n^+-n_0^+) &= -\int_{-\infty}^{0} d\xi\left([v_1+D\kappa b_0^k]\frac{\partial b_0}{\partial\xi} + [v_1+\kappa]\frac{\partial n_0}{\partial\xi}\right) \\ &= v_1[1-n_0^+] + \kappa[D/(k+1)-n_0^+]. \end{aligned} \tag{80}$$

We note that this equation is essentially a type of conservation equation in a weakly curved frame—indeed, it can also be obtained by an analysis similar to the derivation of the conservation equation (26) by adding the two equations (76) and (77) and integrating, ignoring the temporal derivates for a quasistationary front solution in the comoving frame. This is the reason for our earlier remark in Sec. III C that the constant left zero mode $\Psi^{(1)}$ is related to conservation.

The second and third boundary conditions are obtained from the two other adjoint zero modes $\Psi^{(2)}$ and $\Psi^{(3)}$ of $\mathcal{L}^*$, discussed in Sec. III C; the general form is similar to the one shown for a $\bar{\Psi}^{(2)}$ for a particular choice of parameters in Fig. 12, except that the derivative of the *n*-like component does not vanish at $\xi=0$. These zero eigenmodes of $\mathcal{L}^*$ can only be evaluated numerically, but the form of the boundary condition is simply the same for both: with $i=2,3$ we get

$$\begin{aligned} \Psi_2^{(i)}(0)(\nabla_\xi n^+ - \nabla_\xi n_0^+) + \left(v_0\Psi_2^{(i)} - \frac{\partial\Psi_2^{(i)}}{\partial\xi}\Big|_0\right)(n^+-n_0^+) &= -\int_{-\infty}^{0} d\xi\ \ \Psi_1^{(i)}\left([v_1+D\kappa b_0^k]\frac{\partial b_0}{\partial\xi}\right) \\ &\quad -\int_{-\infty}^{0} d\xi\ \ \Psi_2^{(i)}[v_1+\kappa]\frac{\partial n_0}{\partial\xi} \\ &= -v_1\int_{-\infty}^{0} d\xi\ \ \left(\Psi_1^{(i)}\frac{\partial b_0}{\partial\xi} + \Psi_2^{(i)}\frac{\partial n_0}{\partial\xi}\right) \\ &\quad -\kappa\int_{-\infty}^{0} d\xi\ \ \left(\Psi_1^{(i)}Db_0^k\frac{\partial b_0}{\partial\xi} + \Psi_2^{(i)}\frac{\partial n_0}{\partial\xi}\right). \end{aligned} \tag{81}$$

In the sharp interface interpretation, Eqs. (80) and (81) are interpreted as the boundary conditions that relate the change in the local field n_1' and its gradient at the interface (relative to those for a planar moving front) to the local change in velocity of the interface and the local curvature. For a general pattern, the derivative of n_1' with respect to ξ on the left of these equations has to be interpreted as derivative in the direction normal to the interface [40]. As we discussed above, these equations are precisely the three boundary conditions necessary to get, together with the outer equation (72), a well-posed moving boundary problem.

B. Interpretation of the sharp interface formulation

It is useful to pause for a moment to reflect on the structure of the boundary conditions. First of all, note that they all involve terms proportional to the gradient of the nutrient diffusion field, and not to the bacterial density field. The presence of these gradients of the nutrient field on the front side of the interface could have been expected from the numerical observations that the bacterial growth fronts are unstable for small enough *D*. It is well known [7] that such interfacial instability arise for diffusion-limited growth problems where the growth velocity of the interface is proportional to the gradient of the driving field that ''feeds'' the interface. The fact that the gradient of the bacterial field *b* does not appear, makes these bacterial growth fronts most like the so-called ''one-sided crystal growth models,'' describing situations where the diffusion on the backside is absent (e.g., in ''directional solidification,'' the diffusion of impurities in the solid on the backside of the interface is usually negligible in comparison with the diffusion in the liquid on the front side [7]).

We can make this observation more precise as follows. Note that the boundary condition (80), the one that expresses conservation, is the only one that involves Δb^-. Hence we can solve the full dynamical problem by working *only* with

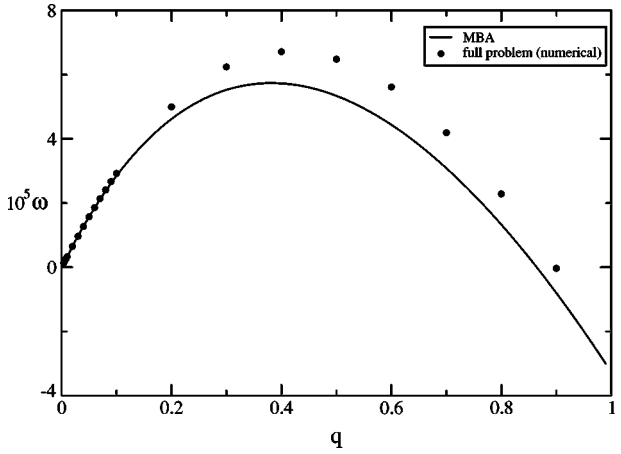

FIG. 13. Comparison between dispersion relation obtained through a sharp interface approach (full line) and through direct numerical linear stability analysis (dots), for the case $k=2$, $D=0.001$. Note that for $q \ll 1$ the results from the moving boundary approximation agree very well with those of the full linear stability calculation, as it should. The reason for the difference between the two curves for q values of order unity is discussed in the text.

the outer n-field and the two boundary conditions (81)—in other words, the outer n-field together with these boundary conditions constitute a closed problem that is sufficient to describe the dynamics of the moving interface. Once this is determined, one can use the conservation condition (80) to determine Δb^- and from there analyze the behavior of the b field on the back with the outer equation (74): *in the sharp interface limit the b* field becomes completely slaved to the interface motion

We already anticipated in Sec. III B that the curvature correction term (the effective surface-tension-like term) should be of order D for small D. This is fully confirmed by our analysis: all the curvature terms in the boundary conditions (80) and (81) either explicitly involve a term D, or a term proportional to n_0 which, as we saw in Sec. II, is proportional to D too for small D.

C. Applicability to the various regimes

The simplest way to test the accuracy of a moving boundary formulation is by comparing the dispersion relation from the moving boundary problem with the dispersion relation obtained from the full model as discussed in Sec. III A. The two outer equations are linear diffusion equations of the standard form, while the boundary conditions are (by construction) also linear. Consequently, the stability of the planar solution of the sharp interface problem follows the standard stability problem as discussed in [7] in which the growth or decay of small single-mode perturbations about the planar interface solution is determined. We will therefore not report it here. In Fig. 13 we illustrate such a comparison for a typical case in the small D regime, where the moving boundary approximation is expected to work best since the diffusion length is in the large nutrient + region. The figure, which is for the case $k=2$ and $D=0.001$ confirms that for small q the dispersion relation of the moving boundary approximation (full curve) essentially lies on top of the one derived from the full problem (symbols). This is as it should be, since for small q clearly $qW \ll 1$, so that condition for the moving boundary approximation to be accurate is fulfilled. The overall shape of the dispersion relation of the moving boundary approximation is actually quite close to the exact one, but for larger q there clearly are some quantitative differences, even for this small value of D. This discrepancy is in our view due to what we discussed before, the fact that the range of unstable wave numbers for this case is finite ($q_c \approx 0.8$), while the interface width W is finite too, so that $q_c W$ does not approach zero as $D \to 0$.

Even though the moving boundary approximation therefore does not become formally correct in this limit (in the sense that the correction terms cannot be made arbitrarily small by taking D sufficiently small), it clearly does quite well in practice for these parameter values. Probably this is due to the fact that W is still relatively small compared to the wavelength $\lambda_c = 2\pi/q_c$ corresponding to the marginal wave number q_c: If we take $W \approx 2$ we get $W/\lambda_c \approx 1/4$, so even though we cannot make this ratio arbitrarily small by sending $D \to 0$, it appears to be small enough in practice to make the sharp interface formulation work well. What may also play a role is that for problems with nonlinear diffusion such as this one, the response of the interfacial zone to perturbations is mostly determined by the rather thin zone where b is small; we have not attempted to substantiate this intuitive idea, however.

A similar observation holds for the time scales. As Fig. 9 illustrates, the maximum growth rate ω_m of the most unstable mode is proportional to D and hence to v_0 for small D; the proportionality $\omega_m \simeq v_0 q_m$ is also consistent with the Mullins-Sekerka dispersion relation (57) discussed in Sec. III A. The internal relaxation time τ_{front} of the front itself is expected to be of order W/v, hence $\omega_m T \simeq q_m W$ remains finite in the limit $D \to 0$: there is no full separation of time scales either.

Also for $k \gg 1$ and D of order unity, the present approximation works generally very well, since on the one hand the diffusion length in the nutrient zone ahead of the front is large (as $v_0 \sim 1/k$ for k large), while on the other hand, the interfacial zone tends to becomes relatively small, even though it does not appear to go to zero—see Fig. 6 and the discussion at the end of Sec. II. We have also investigated the possibility whether in the limit $k \gg 1$ another approximation might be possible, one in which there are three zones, an outer region in front of the interface where $b=0$ as we had above, a very thin zone (of exponentially small width, see Sec. II) where b quickly rises to a value close to 1 while n hardly changes, and a region behind this zone where $\Delta b = b - 1$ is already small and where n decays to zero. We have not been able to make this approximation work to our satisfaction, basically because we have not been able to match the thin zone properly to the region behind it.

For values D and k of order unity, but not too close to the stability boundary $D_c(k)$, the discrepancy between dispersion relation of the moving boundary approximation that we have derived above and the exact dispersion relation is bigger than in Fig. 13 for small D. This is to be expected, since in this limit diffusion length in the outer n region is of the

same order as the interface width, and, moreover, the diffusion in the bacterial region is more important. Nevertheless, the order of magnitude of the growth rate and the range of unstable wave numbers are right.

Finally, we note that since a long-wavelength instability occurs upon decreasing D below $D_c(k)$, we expect that just to the left of this line, the dynamics can be described by the so-called Kuramoto-Sivashinsky equation [41,42]. In fact, since the line $D_c(k)$ is very straight for k larger than 1, the problem may well simplify in the limit $D\to\infty$, $k\to\infty$, D/k fixed. We have not attempted to study this limit or to give an explicit derivation of the Kuramoto-Sivashinksky equation near the boundary.

V. SUMMARY AND OUTLOOK

We have shown that a nonlinear diffusion coefficient and a simple bilinear autocatalysis is sufficient to generate a long-wavelength instability as long as the diffusion constant obeys $D<D_c$, where D_c depends on the nonlinearity. We hope that these results will be of help in sorting out to what extent the present class of models does describe the real bacterial growth problems. To do so, one would of course have to be able to map the bacterial growth properties onto the effective diffusion coefficient in this model. If this can be done, the clearest test with the aid of the present results would be to see whether the interfacial instability becomes suppressed once the effective bacterial density becomes too large.

It would also be of interest to extend numerical simulations like those of Golding *et al.* [10] and those of Kitsunezaki [22], whose parameter values are indicated by crosses in Fig. 3. As we discussed in the Introduction, these numerical results appear to contradict our analytical results, but this may be due to finite size effects and the limited time of the simulation.

In addition to providing a starting point for further studies of these models for bacterial growth, we have been able to develop a new type of linear stability calculation that applies to the general class of fronts with singular behavior of the fields as a result of nonlinear diffusion. Our methods therefore opens up the possibility to study other systems as well, like the vortex fronts [19,20] we mentioned in the Introduction. In addition we were able to reformulate the reaction diffusion problem with nonlinear diffusion away from the stability boundary $D_c(k)$ in the form of a free boundary-type problem; our analysis shows that in the present model bacterial growth fronts are closest to those described by the so-called one-sided model in the theory of crystal growth [7].

Of course, our results are far from the final answer on these types of bacterial growth models: the knowledge that the planar front is unstable is only the first (though crucial) step towards understanding the actual evolving patterns, which are determined by nonlinear effects. In addition, within the context of understanding the bacterial growth problem, the question remains to what extent models with nonlinear diffusion suffice to capture the important growth dynamics.

Clearly, we have studied only the simplest variant of such models, by leaving out the death term, that appears to be important for the morphology [2,22], as well as lots of effects that are important for a more realistic model for bacterial colony growth, like the sporulation of bacteria already mentioned in the Introduction: Computer simulations have shown that in order that branches can form, the sporulation term $-\mu b$ has to be present in Eq. (6).

We have not tried to study how the critical line $D_c(k)$ approaches the origin as $k\downarrow 0$; this is an interesting technical question, but one that probably is of limited relevance for understanding the bacterial growth problem. In fact, the behavior near the origin in the D-k-phase diagram is very singular and hence sensitive to changes in the model: the nonlinear diffusion as well as finite cutoff effects as well as changing the bilinear reaction term bn to $b^\gamma n$ change the mathematical behavior dramatically.

Finally, we want to draw attention to an open mathematical question—at least for us. In a solvability-type analysis, the boundary conditions one normally imposes on the adjoint fields follow from the requirement that $\langle \Psi(\mathcal{L}\Phi)\rangle = \langle (\mathcal{L}^*\Psi)\Phi\rangle$ for all dynamically relevant functions Φ [see Eq. (63)]. However, in the derivation of our moving boundary approximation, we have operated differently: instead of imposing boundary conditions on the adjoint functions, we have written out the terms from the partial differential equations explicitly, and used the left zero modes on the half space $(-\infty,0]$ that we already knew to obtain the sought for boundary conditions for the physical fields n_1. Clearly, the equations obtained this way follow necessarily from the original differential equations in the weakly curved frame, but this line of reasoning is mathematically different in spirit from the usual Fredholm alternative (solvability theory). We do not know—nor could we find—the mathematical theory behind this approach that appears to be new and very powerful for problems with a singular line.

ACKNOWLEDGMENT

J.M. would like to thank the EU network ''Patterns, Noise, and Chaos'' for financial support.

[1] M. Matsushita, in *Bacteria as Multicellular Organisms*, edited by J. A. Shapiro and M. Dworkin (Oxford University Press, Oxford, 1997).
[2] E. Ben-Jacob, I. Cohen, and H. Levine, Adv. Phys. **49**, 395 (2000).
[3] A. Czirók, in *Fluctuations and Scaling in Biology*, edited by T. Vicsek (Oxford University Press, Oxford, 2001).
[4] H. Fujikawa and M. Matsushita, J. Phys. Soc. Jpn. **58**, 3875 (1989).
[5] I. Rafols, MSc thesis, Chuo University, Japan (1998).
[6] J. Wakita, H. Shimada, H. Itoh, T. Matsuyama, and M. Matsushita, J. Phys. Soc. Jpn. **70**, 911 (2001).

[7] J.S. Langer, Rev. Mod. Phys. **52**, 1 (1980).
[8] E. Ben-Jacob, Contemp. Phys. **34**, 247 (1993).
[9] E. Ben-Jacob, Contemp. Phys. **38**, 205 (1997).
[10] I. Golding, Y. Kozlovsky, I. Cohen, and E. Ben-Jacob, Physica A **260**, 510 (1998).
[11] Y. Kozlovsky, I. Cohen, I. Golding, and E. Ben-Jacob, Phys. Rev. E **59**, 7025 (1999).
[12] A.M. Lacasta, I.R. Cantalapiedra, C.E. Auguet, A. Peñaranda, and L. Ramirez-Piscina, Phys. Rev. E **59**, 7036 (1999).
[13] M. Mimura, H. Sakaguchi, and M. Matsushita, Physica A **282**, 283 (2000).
[14] D.A. Kessler and H. Levine, Nature (London) **394**, 556 (1998).
[15] In technical terms: the fronts in coupled reaction diffusion equations with a linear bacterial diffusion term and a bacterial growth term which is linear in the bacterial density, have so-called ''pulled'' planar fronts that are not unstable. Introducing a small density cutoff as proposed in Ref. [14] makes such fronts weakly ''pushed'' and unstable; introduction of a nonlinear diffusion coefficient of the type proposed by Ben-Jabob and co-workers makes the fronts strongly pushed and also unstable.
[16] L. A. Peletier, in *Application of Nonlinear Analysis in the Physical Sciences*, edited by H. Amman, N. Bazley, and K. Kirchgaessner (Pitman, London, 1981).
[17] J. Bear, *Dynamics of Fluids in Porous Media* (Elsevier, New York, 1972).
[18] G. I. Barenblatt, *Similarity, Self-Similarity and Intermediate Asymptotics* (Consultants Bureau, New York, 1979).
[19] J. Gilchrist, Physica C **291**, 132 (1997).
[20] R. Surdeanu, R.J. Wijngaarden, E. Visser, J.M. Huijbregtse, J.H. Rector, B. Dam, and R. Griessen, Phys. Rev. Lett. **83**, 2054 (1999).
[21] A. Karma and W.-J. Rappel, Phys. Rev. E **57**, 4323 (1998).
[22] S. Kitsunezaki, J. Phys. Soc. Jpn. **66**, 1544 (1997).
[23] S.K. Scott and K. Showalter, J. Phys. Chem. **96**, 8706 (1992).
[24] D. Horvath, V. Petrov, S.K. Scott, and K. Showalter, J. Chem. Phys. **98**, 6332 (1993).
[25] Á. Tóth, D. Horváth, and W. van Saarloos, J. Chem. Phys. **111**, 10964 (1999).
[26] For the case $\gamma=2$ studied in Ref. [25] one finds, e.g., $\beta_c \approx 0.44$.
[27] For $\gamma=1$ and linear diffusion, the fronts are ''pulled,'' meaning that their asymptotic velocity equals the spreading speed v^* of the linearized equations. These fronts are known to be very special, in that perturbation theory does not apply to them (see Ref. [34]). For any $\gamma>1$ but linear diffusion, the linear spreading speed $v^*=0$, and hence fronts in this case have to be pushed. Standard perturbation theory and arguments then apply to them. See Ref. [34] for further discussion of this point.
[28] C. M. Bender and S. A. Orzsag, *Advanced Mathematical Methods for Scientists and Engineers* (McGraw-Hill, New York, 1978).
[29] We note that the system (6),(7) also admits solutions with b decreasing exponentially as $b \propto \exp(-\xi/v_0)$ for $\xi \to \infty$. The existence of such additional solution is quite common for fronts propagating into an unstable state [28]. Typically, such solutions are dynamically irrelevant for initial conditions that are sufficiently localized (e.g., have compact support). The simulations of Ref. [22] indicate that this is also the case here, and we will therefore not investigate such solutions any further.
[30] Although the functions appearing in the stability calculations are effectively only functions of one variable ζ, we prefer to use partial derivatives in this section to stress that we do consider perturbations that depend both on time and on the y variable.
[31] The issue of why fronts are always stable for $k=0$ is quite subtle—compare Ref. [15]. For $k=0$ the fronts are pulled, and then the semi-infinite region ahead of the front determines the dynamics of a front, rather than the nonlinear dynamics within the front region itself. We refer to Ref. [34] for further discussion of this point.
[32] H. Akimoto, R. van Rooijen, R. Jochemsen, G. Frossati, and W. van Saarloos, Phys. Rev. Lett. **85**, 1894 (2000).
[33] The solvability condition for this mode yields $q=0$, while ω is undetermined; hence this mode corresponds to changes in the planer solution. As we have seen in Sec. II, changes in the constants c_b and c_n for the asymptotic behavior of b and n yield planar front solutions with a different velocity. In view of this and the fact (discussed in Sec. IV) that this mode is associated with the conservation law, we assume that this mode does not play a role for perturbations that leave the asymptotic values of c_b and c_n unchanged.
[34] U. Ebert and W. van Saarloos, Phys. Rep. **337**, 139 (2000).
[35] U. Ebert and W. van Saarloos, Phys. Rev. Lett. **80**, 1650 (1998); Physica D **146**, 1 (2000).
[36] P. C. Fife, *Dynamics of Internal Layers and Diffusive Interfaces* (SIAM, Philadelphia, 1988).
[37] We use these terms in the sense of asymptotic matching theory. See, e.g., M. Van Dyke, *Perturbation Methods in Fluid Mechanics* (Parabolic Press, Stanford, 1975).
[38] This is because for $\xi>0$ Ψ_2 of this mode is a constant, and because the n-component of this zero eigenmode is continuous and has a continuous derivative at $\xi=0$.
[39] Since the analysis used to obtain the boundary conditions from the partial integration terms is somewhat nonstandard we stress that the equations derived by taking the inner products with the three adjoint zero modes are clearly necessary conditions. As pointed out also in Sec. V, how the analysis compares to the standard Fredholm alternative (solvability condition) is not quite clear to us.
[40] It is instructive to realize that when we consider a slight shift in the position of a planar front, for the outer field $\partial n_1'/\partial\xi|_0 + v_0 n_1' = 0$, as follows immediately from the outer field solution (16) for the planar case. Thus, the terms on the left-hand side of the above boundary conditions both vanish, and hence both $v_1=0$ and $\kappa=0$, as it should for a shift of a planar front solution.
[41] Y. Kuramoto, *Chemical Oscillations, Waves, and Turbulence* (Springer, New York, 1984).
[42] For a derivation in the context of coupled reaction diffusion equations like the ones considered here, see, e.g., A. Malevanets, A. Careta, and R. Kapral, Phys. Rev. E **52**, 4724 (1995).